Flexible communication between cell assemblies and 'reader' neurons

Céline J. Boucly,[1,*] Marco N. Pompili,[1,2*] Ralitsa Todorova,[1,*]
Eulalie M. Leroux,[1] Sidney I. Wiener,[1] & Michaël Zugaro[1]
[1]Center for Interdisciplinary Research in Biology (CIRB),
Collège de France, CNRS, INSERM, Université PSL, Paris, France
[2]Institut de Psychiatrie et Neurosciences de Paris (IPNP),
INSERM, GHU Psychiatrie Neurosciences, Université de Paris, Paris, France
* These authors contributed equally to this work.
Correspondence should be addressed to M.N.P. (marco.pompili@college-de-france.fr)
or M.Z. (michael.zugaro@college-de-france.fr)

Cell assemblies are considered fundamental units of brain activity, underlying diverse functions ranging from perception to memory and decision-making. Cell assemblies have historically been conceived of as internal representations of specific stimuli or actions. Alternatively, cell assemblies can be endogenously defined by their ability to effectively elicit specific responses in downstream ('reader') neurons. Yet, whether cell assemblies are selectively detected by downstream neurons remains unknown. Here, we provide evidence for such assembly–reader communication. Reader activation was genuinely collective, functionally selective, yet flexible, implementing both pattern separation and completion. These processes occurred at the time scale of membrane integration, synaptic plasticity and gamma oscillations. Finally, assembly–reader couplings were selectively modified upon learning, indicating that they were plastic and reflected behaviorally relevant variables. These results support cell assemblies as an endogenous mechanism for brain function.

An increasingly influential hypothesis in neuroscience posits that 'cell assemblies' are computational units of the brain that can mediate complex information processing beyond the aggregate power of single cells (*1–10*). Cell assemblies have often been conceived of in relation to external stimuli or motor activity (a 'representational' framework), with the underlying assumption that assembly members can code for complementary features that become bound through synchronous activation (*11–13*). However, this theoretical framework cannot be readily extended to higher order cortical areas, where assemblies (*10, 14–19*) cannot be assessed in terms of known sensory or motor correlates, and where represented entities are ill defined and notoriously difficult to test. More fundamentally, epistemological arguments (*20, 21*) suggest that even features that experimenters tentatively assign to assembly members (such as color and shape) may not be purely objective characteristics of external items, but may at least in part result from endogenous properties of the brain itself. Accordingly, seeking objective features represented in cell assemblies could constitute a circular problem. An alternative approach to study cell assemblies is by focusing on brain processes, and considering the effects of assemblies on downstream 'reader' neurons. In this 'reader-centric' framework (*22*), a cell assembly can be characterized by its ability to trigger a specific response in one or more target neurons, underlying specific autonomic, behavioral or cognitive functions. However, whether this appealing definition is supported by physiological evidence remains an open question, possibly because of technological limitations even in state-of-the-art causal technologies. Indeed, current approaches, including timed and targeted optogenetics, do not yet permit selective and thorough manipulation of defined groups of neurons at the precise moment when they are about to form specific cell assemblies, but not when they fire individually.

An alternative approach to test this conceptual framework is to identify putative cell assemblies and downstream 'reader' neurons during endogenous (non-representational) brain activity, and then show that learning and memory results in selective and predictable changes in assembly–reader relations. For

this, we recorded from large neuronal ensembles in two reciprocally interconnected associative brain areas, namely the cortico-amygdalar circuit (Fig. 1a) (*23*). We first examined collective neural dynamics during sleep, when brain activity is dominated by endogenous processes and is not directly representational. Cell assemblies were identified using a PCA-ICA algorithm (*24*) (see Methods). Note that this identification method only relies on spike train statistics, but does not require attribution of additional functional properties posited by the respective conceptual frameworks, i.e. feature coding or effective spike transmission. In each sleep session, groups of prefrontal units recurrently fired with high synchrony, forming cell assemblies (*15–18*) (Fig. 1b,c, median $n = 18$; Fig. S1a,c–e). As expected, cells participating in assemblies ('members') fired more synchronously with each other than with non-members, and their spike trains could be reliably predicted from those of other members of the same assembly ('peer prediction', (*14*); Fig. 1b). While cell assemblies have been primarily studied in cortical areas (see e.g. (*25*)), synchronous activity patterns have been reported in subcortical structures (*10, 26–28*). We thus tested and confirmed (*29*) that amygdalar neurons also formed cell assemblies (Fig. 1b,d, Fig. S1b–e). Similar to the prefrontal cortex, synchrony and peer prediction were significantly greater than expected by chance. This is consistent with the notion that cell assemblies are a general brain mechanism extending beyond cortical areas (*10, 26, 28*).

According to the 'reader-centric' framework, assemblies should effectively elicit discharges in downstream reader neurons. This has two implications: first, activation of an assembly should precede that of its reader within a brief time window, occurring more frequently than expected by chance; and second, this relationship should be dependent on the *collective* activation of the assembly.

We first investigated whether cell assemblies reliably triggered spiking in downstream neurons. We sought occurrences of prefrontal assembly activations closely followed (10–30 ms, (*30*)) by spiking in single amygdalar neurons. In 347 candidate assembly–reader pairs (Fig. 1e,f) this temporal coordination was greater than expected by chance ($p<0.05$, Monte-Carlo bootstrap). Conversely, in 502 cases, amygdalar assembly activations were consistently followed by prefrontal spikes ($p<0.05$, Monte-Carlo bootstrap; Fig. 1e,f; see also Fig. S2). Downstream neurons were more likely to discharge when increasing numbers of members were active together (Fig. S3), consistent with the hypothesis that it is the synchronous activation of a cell assembly that drives responses in reader neurons.

Second, to assess whether spiking in downstream neurons was actually selective for the collective activation of upstream assemblies, we sought to rule out two confounding scenarios: 1) downstream neurons could be merely responding to each of the assembly members independently, and 2) they could be responding to the compound activation of the assembly (excitatory drive), irrespective of the precise identity of participating members.

We first verified that assembly members exerted a synergistic, rather than independent (linearly summating), influence on their targets. In one extreme scenario, one or two 'vocal' members might suffice to evoke maximal discharge in the target neuron while the other members would not have any impact on the response. To rule out this possibility, we discarded all assembly activations in which the most effective members were active. In the remaining cases, the responses of the target neurons remained well above their baseline firing rates (Fig. 2a; Fig. S4). To further address this scenario in its most general form, we trained a generalized linear model (GLM) to predict reader activity from the spikes of the respective assembly members outside assembly activation epochs. We then used this pre-trained GLM to predict responses to assembly activations. This estimated how the reader would respond if it were processing each of its inputs independently. The observed response to assembly activations exceeded this linear estimate and peaked at a delay of ∼20 ms (Fig. 2b; Fig. S5), indicating that the collective activation of assembly members was capable of evoking greater responses than the sum of their individual contributions.

We then assessed whether members were interchangeable, or even dispensable, provided their total spike count remained the same. To test for this, for any given pair of assembly members (A and B), we compared reader responses when each of the two members emitted exactly one spike (AB) vs when only one of the two members emitted exactly two spikes (AA), thus maintaining a constant number of assembly spikes while blurring cell identity. This analysis revealed that the identity of participating members mattered beyond their compound activity (Fig. 2c, Fig. S6). This is consistent with the hypothesis that the response of the reader neuron should depend on detailed spatio-temporal properties of its inputs (e.g. precisely timed spike patterns impinging on specific combinations of dendritic branches (*31*)).

These results are consistent with the prediction that assemblies exert a collective impact on their readers. To investigate the time scale of this synergistic effect, we repeated these analyses for varying interspike

intervals and assembly durations. Both approaches yielded results consistent with an endogenous time scale of up to ∼20-25 ms for effective cell assemblies (Fig. 2c, Fig. S7, and Fig. S8). This time scale corresponds to those of functionally relevant cellular and network properties, including membrane integration time constants and local delays (*32*), optimal time windows for spike timing dependent potentiation of synaptic efficacy (*33*), and the period of synchronizing gamma oscillations (*34*).

Note that a given assembly could drive multiple reader neurons which may very well, in turn, participate in cell assemblies. Indeed, in the amygdala 82 readers (out of 204) did participate in 147 assemblies, 42 of which were detected by prefrontal readers. Further, compared to other amygdalar neurons, amygdalar readers were significantly more likely to participate in cell assemblies targeting prefrontal readers (p=1.2e-4, chi-square test). Similarly, 278 (out of 404) prefrontal readers participated in 247 assemblies, 104 of which triggered amygdalar readers, and thus were significantly more likely than other prefrontal neurons to target amygdalar readers (p=2.6e-21, chi-square test). This is consistent with the notion that cell assemblies can be detected by cell assemblies, extending the concept of reader neurons and providing a generalized mechanism for bidirectional communication.

We next investigated computational and functional properties of the assembly–reader mechanism. Does assembly reading manifest pattern completion (similar reader responses upon activation of a sufficient subset of assembly members) and pattern separation (discrimination between partially overlapping assemblies)? To test for pattern completion, we assessed reader responses following partial activation of upstream assemblies, and measured how they increased with the number of active members. Reader responses did not simply increase proportionally to the number of active members but were significantly better fit by a sigmoid curve, thus providing evidence for pattern completion (*35*) (Fig. 3a, Fig. S9). Regarding pattern separation, we first compared the activity of readers following activation of each of the simultaneously recorded assemblies, and confirmed that reader responses were highly selective for specific assemblies (Fig. 3b, Fig. S10). We then focused on cell assemblies with multiple ($\geq 25\%$) common members, and found that reader neurons effectively discriminated between such overlapping assemblies, providing further evidence for pattern separation (Fig. 3c, Fig. S11). Thus, the assembly–reader mechanism is both robust and selective, since it can implement both pattern completion and pattern separation.

Having identified assembly–reader pairs and found evidence for two of their widely posited computational properties, namely pattern separation and completion, we set out to test the prediction that their relation should be altered by learning and memory in a selective and predictable manner. We compared assembly–reader pairs before and after a standard fear conditioning and extinction protocol known to recruit the prefronto-amygdalar circuit (*36–39*) (Fig. 4a; see Methods). During fear conditioning and subsequent sleep, fear-related signals would be expected to flow from the amygdala to the prefrontal cortex (*40*). We thus examined prefrontal reader responses to amygdalar assemblies, and compared activity during sleep preceding vs following training, when reactivation of cell assemblies has been shown to mediate memory consolidation (*16, 19, 41*). We found numerous examples of amygdalar cell assemblies that were active in both sleep sessions, but formed novel associations with downstream prefrontal neurons following fear conditioning (Fig. 4a). Other downstream prefrontal neurons no longer responded significantly to amygdalar cell assemblies in post-conditioning sleep (Fig. 4a).

To confirm that these changes were specifically related to fear learning as opposed to e.g. exploratory activity, we compared them to changes before and after a control session where no fearful stimuli were provided. Fear conditioning was followed by significantly greater responses in prefrontal readers to amygdalar assemblies (Fig. 4b). Further, in contrast to fear conditioning, fear extinction did not result in such changes (Fig. S12a), indicating that variations in assembly–reader relations were not broadly elicited by general fearful behavior, but rather reflected the specific process of forming new fear memories.

Conversely, during fear extinction, the prefrontal cortex would be expected to alter amygdalar signals (*30*). Consistent with this, the relation between prefrontal assemblies and amygdalar readers underwent substantial reorganization following fear extinction (Fig. 4c). Again, this was specific to this particular cognitive process, since fear conditioning did not yield changes in assembly-reader pairs significantly different from control sessions (Fig. S12b).

Our results indicate that single neurons in downstream structures can reliably and selectively respond to the activation of upstream cell assemblies. The responses were stronger than expected for the sum of independent inputs, and depended on the identity of the participating neurons rather than their aggregate drive. The process therefore implemented a genuinely collective computation, and supports a possible alternative, operational, rather than representational, definition for cell assemblies (*22*), without reference

to features of external stimuli or actions (*8*). Individual neurons could be involved in both cell assembly and reader functions, suggesting that the readout of cell assemblies was not only performed by isolated neurons, but more generally by other cell assemblies as well (*42, 43*), which would then communicate with cell assemblies in other areas. In addition, because a fraction of the members were sufficient to elicit reader responses, yet readers discriminated between partly overlapping assemblies, the process implemented both pattern separation and pattern completion (*1, 44*). Finally, flexible functional changes in assembly–reader pairing emerged during learning. Using fear conditioning and extinction as a model, we showed that assembly–reader relations selectively changed during learning in a behaviorally-relevant manner, supporting the role of cell assemblies as functional units of brain computation.

Acknowledgments

We thank G. Makdah for help with data acquisition and Y. Dupraz for technical support. This project was funded by the Agence Nationale de la Recherche (ANR-17-CE37-0016-01) (M.Z.), Labex MemoLife (ANR-10-LABX-54 MEMO LIFE, ANR-10-IDEX-0001-02 PSL*) (M.N.P. and S.I.W.), French Ministry of Research (C.B.), and Collège de France (R.T.) The authors declare no competing interests. Research design: C.J.B., M.N.P., R.T., S.I.W., M.Z. Experiments: E.M.L., M.N.P. Data analysis design: C.J.B., M.N.P., R.T., S.I.W., M.Z. Data analysis: C.B.J., R.T. Manuscript: C.B.J., M.N.P., R.T., S.I.W., M.Z.

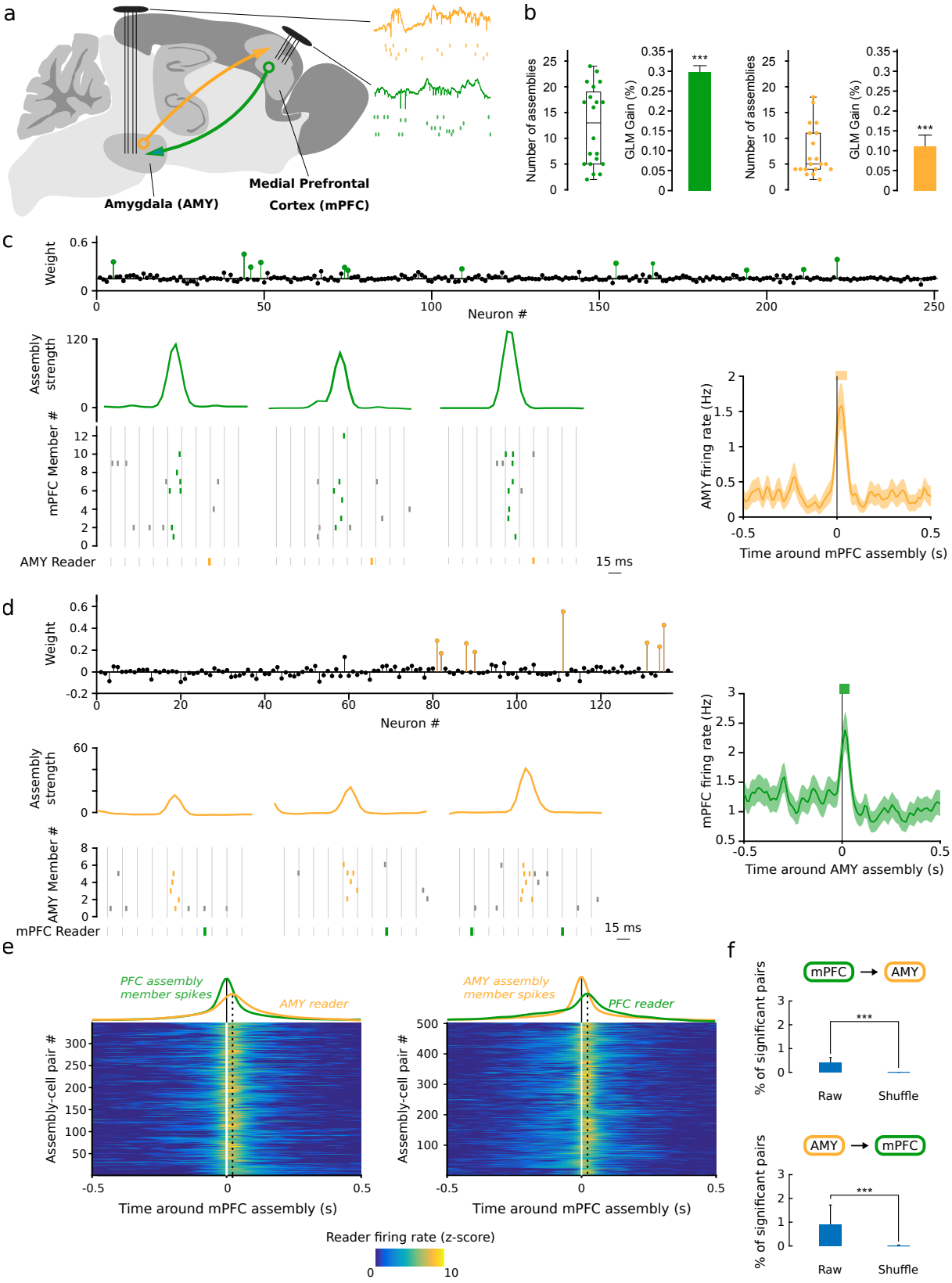

Fig. 1. Cell assembly activations are closely followed by downstream spiking. **a**, Simultaneous high-densisty recordings in the bi-directionally connected medial prefrontal cortex and amygdala ($n = 4$ rats; 5 sessions each). **b**, Numbers of assemblies in prefrontal (left, median $N = 13$) and amygdalar (right, median $N = 5$) recordings in individual sessions (boxes and whiskers: distribution quartiles). Median ± s.e.m. peer prediction of the activity of assembly members from other members (gain relative to shuffled data, ***p<0.001; Wilcoxon rank sum test).

continued →

Fig. 1 (continued). **c**, Example medial prefrontal cortical assembly activations closely (10–30 ms) followed by significant responses of an amygdalar neuron. Top: cell assembly weights (colored circles: assembly members, black circles: non-members). Bottom left: examples of assembly activation (curves: activation strength) followed by downstream spiking (rasters: prefrontal spikes within (green) and outside (gray) epochs of assembly activation; orange rasters: amygdalar spikes). Right: firing rate of amygdalar neuron centered on all prefrontal assembly activations (mean $\pm$ s.e.m.). Thick orange horizontal bar indicates significant responses ($p<0.05$: Monte-Carlo bootstrap test; see Methods). **d**, Same as (**c**) for amygdalar assembly and downstream prefrontal neuron. **e**, Average downstream responses (z-scored firing rates) centered on assembly activations, over all significant pairs (color plots), and averaged across pairs (color curves) compared with the average activity of the upstream assembly. Left: prefrontal assemblies and amygdalar downstream neurons. Right: amygdalar assemblies and downstream prefrontal neurons. **f**, Percentage of significant assembly-reader pairs found in shuffled recordings vs. real data (***$p<0.001$, Wilcoxon signed-rank test).

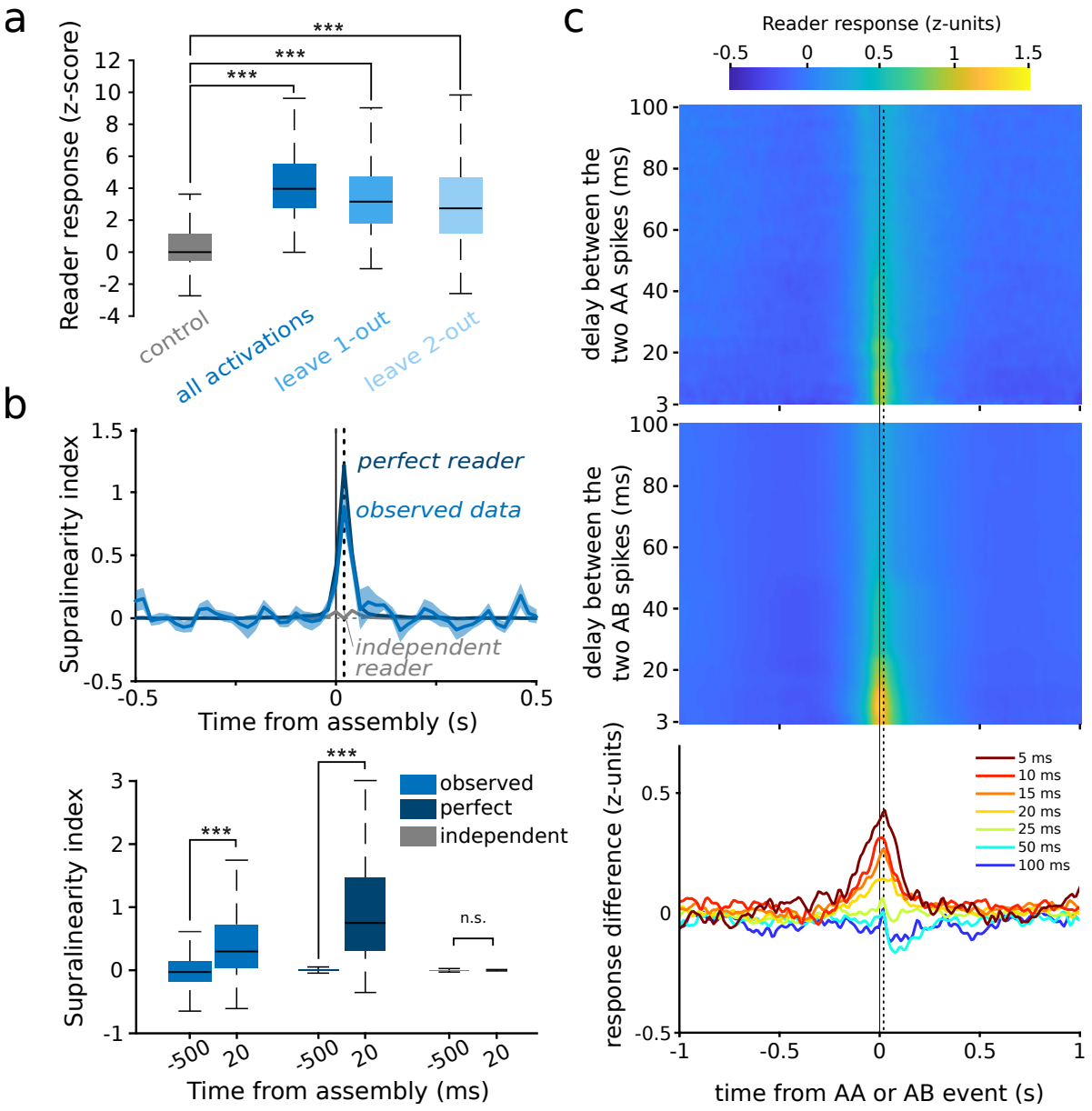

Fig. 2. Readers respond to the collective activity of assemblies. **a**, Average response of reader neurons to upstream assembly activations when the most effective members of upstream assemblies were not recruited. As a control, assemblies and downstream neurons were taken randomly among non-significant pairs. **b**, Supralinearity of reader responses to the collective activity of assembly members. Top: Supralinearity index of data (blue curve) compared to a simulated perfect collective reader (dark blue curve) and to a simulated independent reader (gray curve). Bottom: Supralinearity index 20 ms after assembly activations was significantly greater than at baseline (500 ms prior to assembly activations) for both the observed data (***$p<0.001$, Wilcoxon signed-rank test) and the simulated perfect collective readers (***$p<0.001$, Wilcoxon signed-rank test), but not for the simulated independent readers ($p=0.7916$, Wilcoxon signed-rank test). **c**, Top: mean z-scored responses of reader neurons to two successive spikes of the same member (AA) of an upstream assembly as a function of the temporal delay between the two spikes. Center: same as top, but for reader responses to two successive spikes of two different assembly members (AB). Bottom: difference between the two (AB−AA), for varying temporal delays. The response to co-activations of different members (AB) is greater than the response to multiple activations of the same member (AA) only for brief (<25 ms) delays between spikes (***$p<0.001$, Wilcoxon signed-rank test). Vertical dashed lines indicate 20 ms.

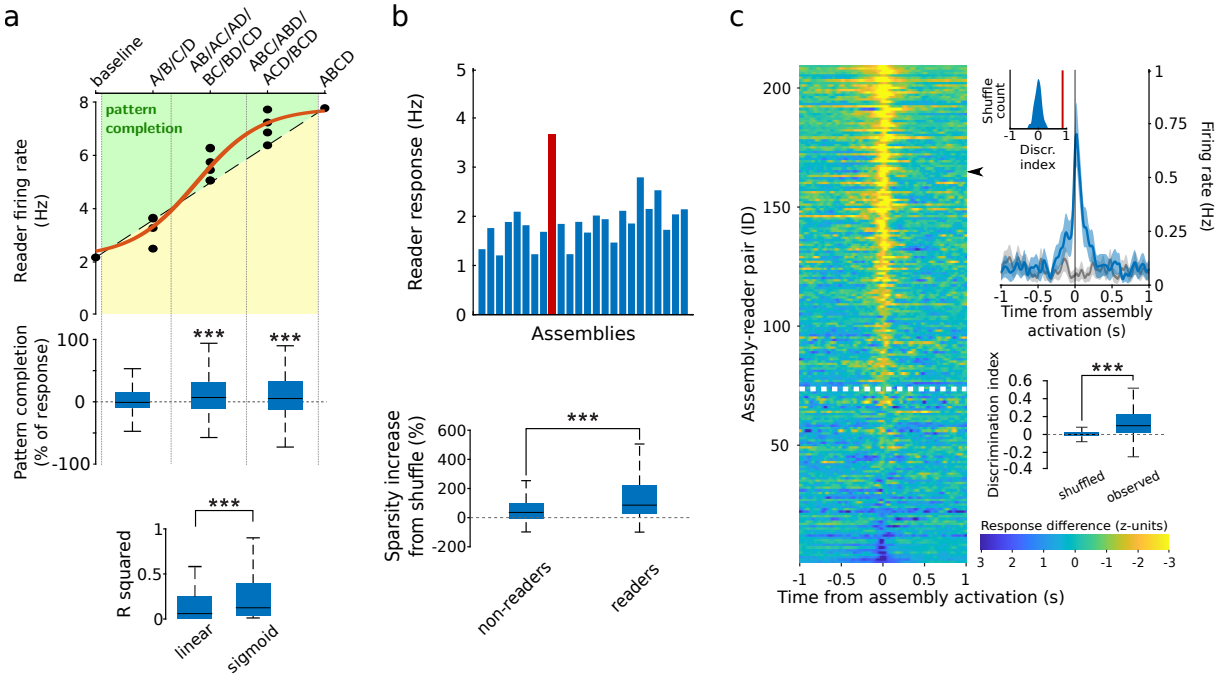

Fig. 3. Computational properties of the assembly–reader mechanism. a, Pattern completion. Response of one example reader to incomplete activations of a 4-member assembly (ABCD). Dashed line: proportional response. Red curve: best-fit sigmoid. Green zone: pattern completion. Center: boost in reader response (relative to a proportional response) for all assembly–reader pairs as a function of the number of active assembly members. The gain was significant for the second and third quantiles (***$p<0.001$, Wilcoxon signed-rank test). Bottom: Proportional vs sigmoidal fits of observed data (***$p<0.001$, Wilcoxon signed-rank test). **b**, Pattern separation. Top: responses of an example reader neuron to each cell assembly detected in the same session (red bar: specific assembly read by this downstream neuron). Bottom: sparsity (increase relative to shuffled data) of the responses of reader neurons to assembly activations was significantly greater than shuffled data ($p<0.001$, Wilcoxon signed rank test) and than responses of non-reader neurons (***$p<0.001$, Wilcoxon rank sum test). **c**, Pattern separation. Left: Mean difference between reader responses to activations of paired assemblies and other assemblies with overlapping members ($\geq 25\%$ of all members). Data are sorted by discrimination index. Responses above the white dotted line displayed significant pattern separation (discrimination index greater than 95% of the shuffled data). Top right: response of an example reader (black arrow) to its paired assembly (blue curve) vs to another assembly with overlapping members (gray curve) (mean $\pm$ s.e.m.). Bottom right: Observed discrimination indices were greater than the discrimination indices for shuffled data (***$p<0.001$, Wilcoxon rank sum test).

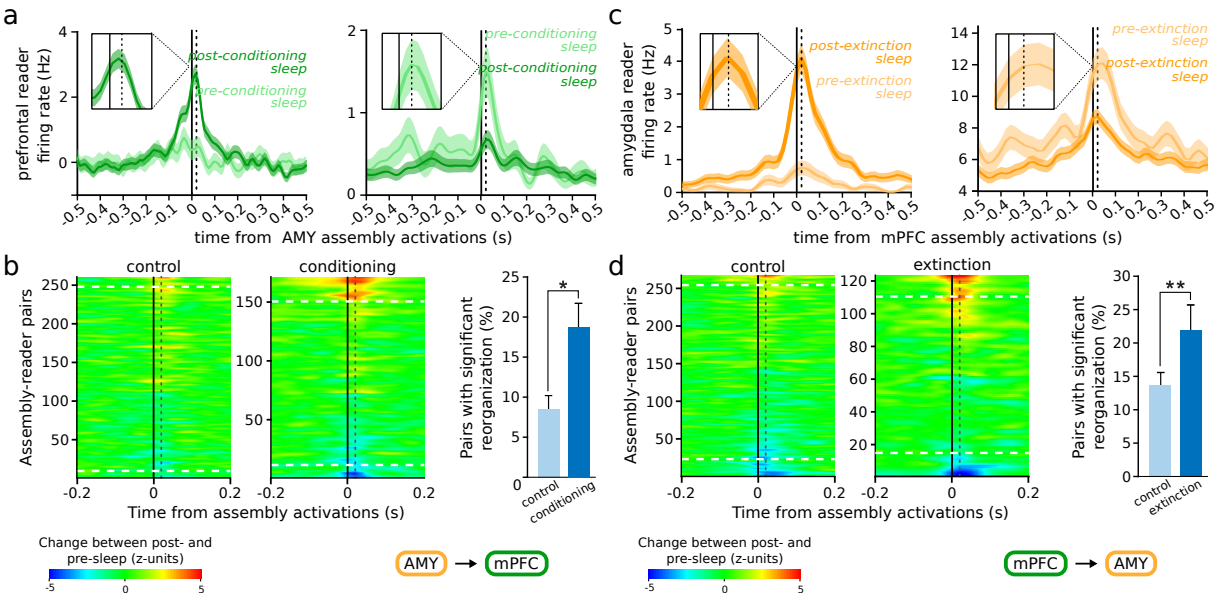

Fig. 4. Learning-related changes in assembly–reader relations. **a**, Examples of a reader increasing (left) or decreasing (right) their responses (shaded area: mean ± s.e.m.) to assembly activations before (light green) and after (green) fear conditioning. Dotted line: 20 ms. **b**, Left: Responses of a prefrontal reader between post and pre sleep, centered on amygdalar assembly activations. Data are sorted according to response magnitudes. Assembly–reader pairs above the higher dashed line (resp. below the lower dashed line) significantly ($p<0.05$, Monte-Carlo bootstrap test) increased (resp. decreased) their responses in post-task sleep. Right: More assembly–reader pairs significantly changed their responses ($p<0.05$, Monte-Carlo bootstrap test) following fear conditioning than following control sessions (*$p=0.0149$, chi-square test). **c**, Left: Same as (**a**) for example amygdalar reader responses to prefrontal assemblies following fear extinction. **d**, Left: Same as (**b**) for amygdalar reader responses to prefrontal assemblies following control sessions vs fear extinction sessions. Right: More assembly–reader pairs significantly changed their response ($p<0.05$, Monte-Carlo bootstrap test) after fear extinction than after control sessions (**$p=0.0056$, chi-square test).

References

1. D. O. Hebb. *The Organization of Behavior*. Wiley, 1949.
2. H. B. Barlow. Single units and sensation: A neuron doctrine for perceptual psychology? *Perception*, 1(4):371–394, 1972.
3. V. Braitenberg. Cell Assemblies in the Cerebral Cortex. In *Theoretical Approaches to Complex Systems*, pages 171–188. Springer, Berlin, Heidelberg, 1978.
4. J. J. Hopfield. Neural networks and physical systems with emergent collective computational abilities. *PNAS*, 79(8):2554–2558, 4 1982.
5. A. Pouget, P. Dayan, and R. Zemel. Information processing with population codes. *Nature Reviews Neuroscience*, 1(2):125–132, 2000.
6. F. Varela, J. P. Lachaux, E. Rodriguez, and J. Martinerie. The brainweb: Phase synchronization and large-scale integration. *Nature Reviews Neuroscience*, 2(4):229–239, 2001.
7. K. D. Harris. Neural signatures of cell assembly organization. *Nature Reviews Neuroscience*, 6(5):399–407, 2005.
8. H. Eichenbaum. Barlow versus Hebb: When is it time to abandon the notion of feature detectors and adopt the cell assembly as the unit of cognition? *Neuroscience Letters*, 680:88–93, 2018.
9. M. El-Gaby, H. M. Reeve, V. L. dos Santos, N. Campo-Urriza, P. V. Perestenko, A. Morley, L. A. M. Strickland, I. P. Lukács, O. Paulsen, and D. Dupret. An emergent neural coactivity code for dynamic memory. *Nature Neuroscience*, 2021.
10. V. J. Oberto, C. J. Boucly, H. Gao, R. Todorova, M. Zugaro, and S. I. Wiener. Distributed cell assemblies spanning prefrontal cortex and striatum. *Current Biology*, 32(1):1–13.e6, 2021.
11. C. von der Malsburg. The correlation theory of brain function. In *Internal Report 81-2*. Dept. of Neurobiology, Max-Planck-Institute for Biophysical Chemistry, Göttingen, Germany, 1981.
12. A. P. Georgopoulos, A. B. Schwartz, and R. E. Kettner. Neuronal population coding of movement direction. *Science*, 233(4771):1416 – 1419, 1986.
13. C. M. Gray, P. König, A. K. Engel, and W. Singer. Oscillatory responses in cat visual cortex exhibit inter-columnar synchronization which reflects global stimulus properties. *Nature*, 338(6213):334 – 337, 1989.
14. K. D. Harris, J. Csicsvari, H. Hirase, G. Dragoi, and G. Buzsáki. Organization of cell assemblies in the hippocampus. *Nature*, 424(6948):552–556, 7 2003.
15. S. Fujisawa, A. Amarasingham, M. T. Harrison, and G. Buzsáki. Behavior-dependent short-term assembly dynamics in the medial prefrontal cortex. *Nature Neuroscience*, 11(7):823–833, 7 2008.
16. A. Peyrache, M. Khamassi, K. Benchenane, S. I. Wiener, and F. P. Battaglia. Replay of rule-learning related neural patterns in the prefrontal cortex during sleep. *Nature Neuroscience*, 12(7):919–926, 2009.
17. K. Benchenane, A. Peyrache, M. Khamassi, P. L. Tierney, Y. Gioanni, F. P. Battaglia, and S. I. Wiener. Coherent theta oscillations and reorganization of spike timing in the hippocampal-prefrontal network upon learning. *Neuron*, 66(6):921–936, 6 2010.
18. C. Dejean, J. Courtin, N. Karalis, F. Chaudun, H. Wurtz, T. C. Bienvenu, and C. Herry. Prefrontal neuronal assemblies temporally control fear behaviour. *Nature*, 535(7612):420–424, 7 2016.
19. R. Todorova and M. Zugaro. Isolated cortical computations during delta waves support memory consolidation. *Science*, 366(6463):377–381, 10 2019.
20. H. R. Maturana and F. J. Varela. *The tree of knowledge: The biological roots of human understanding.* New Science Library/Shambhala Publications, 1987.
21. G. Buzsáki. *The brain from inside out.* Oxford University Press, 2019.

22. G. Buzsáki. Neural Syntax: Cell Assemblies, Synapsembles, and Readers. *Neuron*, 68(3):362–385, 11 2010.

23. C. J. Reppucci and G. D. Petrovich. Organization of connections between the amygdala, medial prefrontal cortex, and lateral hypothalamus: a single and double retrograde tracing study in rats. *Brain Structure and Function*, 221(6):2937–2962, 7 2016.

24. V. Lopes dos Santos, S. Ribeiro, and A. B. Tort. Detecting cell assemblies in large neuronal populations. *Journal of Neuroscience Methods*, 220(2):149–166, 11 2013.

25. K. D. Harris. Cell assemblies of the superficial cortex. *Neuron*, 76(2):263–265, 2012.

26. C. M. Pennartz, E. Lee, J. Verheul, P. Lipa, C. A. Barnes, and B. L. McNaughton. The ventral striatum in off-line processing: Ensemble reactivation during sleep and modulation by hippocampal ripples. *Journal of Neuroscience*, 24(29):6446–6456, 7 2004.

27. L. Sjulson, A. Peyrache, A. Cumpelik, D. Cassataro, and G. Buzsáki. Cocaine Place Conditioning Strengthens Location-Specific Hippocampal Coupling to the Nucleus Accumbens. *Neuron*, 98(5):926–934, 6 2018.

28. H. Miyawaki and K. Mizuseki. De novo inter-regional coactivations of preconfigured local ensembles support memory. *Nature communications*, 13(1):1–21, 2022.

29. K. M. Gothard. Multidimensional processing in the amygdala. *Nature Reviews Neuroscience*, 21(10):565 – 575, 2020.

30. E. Likhtik, J. G. Pelletier, R. Paz, and D. Paré. Prefrontal control of the amygdala. *Journal of Neuroscience*, 25(32):7429 – 7437, 2005.

31. T. Branco, B. A. Clark, and M. Häusser. Dendritic discrimination of temporal input sequences in cortical neurons. *Science*, 329(5999):1671 – 1675, 2010.

32. C. Koch, M. Rapp, and I. Segev. A brief history of time (constants). *Cerebral Cortex*, 6(2):93–101, 1996.

33. G. Q. Bi and M. M. Poo. Synaptic modifications in cultured hippocampal neurons: Dependence on spike timing, synaptic strength, and postsynaptic cell type. *Journal of Neuroscience*, 18(24):10464–10472, 12 1998.

34. G. Buzsáki and E. W. Schomburg. What does gamma coherence tell us about inter-regional neural communication? *Nature Neuroscience*, 18(4):484 – 489, 2015.

35. J. L. McClelland and N. H. Goddard. Considerations arising from a complementary learning systems perspective on hippocampus and neocortex. *Hippocampus*, 6(6):654 – 665, 1996.

36. M. A. Morgan and J. E. LeDoux. Differential contribution of dorsal and ventral medial prefrontal cortex to the acquisition and extinction of conditioned fear in rats. *Behavioral Neuroscience*, 109(4):681, 1995.

37. J. Muller, K. P. Corodimas, Z. Fridel, and J. E. LeDoux. Functional inactivation of the lateral and basal nuclei of the amygdala by muscimol infusion prevents fear conditioning to an explicit conditioned stimulus and to contextual stimuli. *Behavioral Neuroscience*, 111(4):683–682, 1997.

38. C. Herry, S. Ciocchi, V. Senn, L. Demmou, C. Müller, and A. Lüthi. Switching on and off fear by distinct neuronal circuits. *Nature*, 454(7204):600–606, 2008.

39. D. Sierra-Mercado, N. Padilla-Coreano, and G. J. Quirk. Dissociable roles of prelimbic and infralimbic cortices, ventral hippocampus, and basolateral amygdala in the expression and extinction of conditioned fear. *Neuropsychopharmacology*, 36(2):529–538, 1 2011.

40. D. Popa, S. Duvarci, A. T. Popescu, C. Léna, and D. Paré. Coherent amygdalocortical theta promotes fear memory consolidation during paradoxical sleep. *PNAS*, 107(14):6516–6519, 2010.

41. G. Girardeau, I. Inema, and G. Buzsáki. Reactivations of emotional memory in the hippocampus-amygdala system during sleep. *Nature Neuroscience*, 20(11):1634–1642, 2017.

42. M. Abeles. *Local Cortical Circuits*. Studies of Brain Function. Springer Berlin Heidelberg, 1982.

43. Y. Ikegaya, G. Aaron, R. Cossart, D. Aronov, I. Lampl, D. Ferster, and R. Yuste. Synfire chains and cortical songs: Temporal modules of cortical activity. *Science*, 304(5670):559 – 564, 2004.

44. A. Lansner and E. Fransen. Modelling hebbian cell assemblies comprised of cortical neurons. *Network*, 3(2):105 – 119, 1992.

45. M. O. Pasquet, M. Tihy, A. Gourgeon, M. N. Pompili, B. P. Godsil, C. Léna, and G. P. Dugué. Wireless inertial measurement of head kinematics in freely-moving rats. *Scientific Reports*, 6:35689, 2016.

46. M. Pachitariu, N. A. Steinmetz, S. N. Kadir, M. Carandini, and K. D. Harris. Fast and accurate spike sorting of high-channel count probes with kilosort. In D. Lee, M. Sugiyama, U. Luxburg, I. Guyon, and R. Garnett, editors, *Advances in Neural Information Processing Systems*, volume 29. Curran Associates, Inc., 2016.

47. L. Hazan, M. Zugaro, and G. Buzsáki. Klusters, NeuroScope, NDManager: A free software suite for neurophysiological data processing and visualization. *Journal of Neuroscience Methods*, 155(2):207–216, 2006.

48. M. N. Pompili and R. Todorova. Discriminating sleep from freezing with cortical spindle oscillations. *Frontiers in Neural Circuits*, 16, 2022.

49. G. Paxinos and C. Watson. *The Rat Brain in Stereotaxic Coordinates*. Academic Press, 2013.

50. V. A. Marčenko and L. A. Pastur. Distribution of eigenvalues for some sets fo random matrices. *Mathematics of the USSR-Sbornik*, 1(4):457–483, 4 1967.

51. N. Otsu. Threshold selection method from gray-level histograms. *IEEE Transactions on Systems, Man, and Cybernetics*, SMC-9(1):62–66, 1979.

52. G. Rothschild, E. Eban, and L. M. Frank. A cortical-hippocampal-cortical loop of information processing during memory consolidation. *Nature Neuroscience*, 20(2):251–259, 2 2017.

Animals

Four male Long-Evans rats (350–400 g at the time of surgery) were housed individually in monitored conditions (21°C and 45% humidity) and maintained on a 12h light – 12h dark cycle. In order to avoid obesity, food was restricted to 13–16 g of rat chow per day, while water was available *ad libitum*. To habituate the rats to human manipulation, they were handled each workday. All experiments conformed to the approved protocols and regulations of the local ethics committee (Comité d'éthique en matière d'expérimentation animale Paris Centre et Sud n°59), the French Ministries of Agriculture, and Research.

Surgery

The rats were deeply anesthetized with ketamine-xylazine (Imalgene 180 mg/kg and Rompun 10 mg/kg) and anesthesia was maintained with isoflurane (0.1-1.5% in oxygen). Analgesia was provided by subcutaneous injection of buprenorphine (Buprecaire, 0.025 mg/kg) and meloxicam (Metacam, 3 mg/kg). The animals were implanted with a custom built microdrive (144–252 channels) carrying 24, 32, or 42 independently movable hexatrodes (bundles of 6 twisted tungsten wires, 12 µm in diameter, gold-plated to ∼200 kΩ). The electrode tips were typically implanted 0.5 mm above the (bilateral) target brain regions. Miniature stainless steel screws were implanted above the cerebellum to serve as electrical reference and ground.

During recovery from surgery (minimum 7 days), the rats received antibiotic (Marbofloxacine, 2 mg/kg) and analgesic (Meloxicam, 3 mg/kg) treatments via subcutaneous injections and were provided with food and water *ad libitum*. The recording electrodes were then progressively lowered until they reached their targets and adjusted to optimize yield and stability.

Data acquisition and processing

Brain activity was recorded using a 256-channel digital data acquisition system (KJE-1001, Amplipex, Szeged, Hungary). The signals were acquired with four 64-channel headstages (Amplipex HS2) and sampled wideband at 20,000 Hz. An inertial measurement unit (IMU, custom-made non-wireless version of the one described in (*45*)) sampled the 3D angular velocity and linear acceleration of the head at 300 Hz. To determine the instantaneous position of the animal, a red LED mounted on the headstage was imaged by overhead webcams at 30 Hz. Animal behavior was also recorded at 50 Hz by lateral video cameras (acA25000, Basler). Off-line spike sorting was performed using KiloSort (*46*) for prefrontal units, and KlustaKwik (K.D. Harris, `http://klustakwik.sourceforge.net`) for amygdalar units. The resulting clusters were visually inspected using Klusters (*47*) to reject noise and to merge erroneously split units. Neurophysiological and behavioral data were explored using NeuroScope (*47*). LFPs were derived from wideband signals by downsampling all channels to 1250 Hz.

Scoring of behavioral and brain states Automatic detection of immobility was performed by thresholding the angular speed calculated from gyroscopic data as described in (*45*). LFP data was visualized using Neuroscope (*47*) and slow-wave sleep (SWS) was detected as previously described (*48*).

Histological identification of recording sites At the end of the experiments, recording sites were marked with small electrolytic lesions (∼20 µA for 20 s, one lesion per bundle). After a delay of at least three days to permit glial scarring, rats were deeply anesthetized with a lethal dose of pentobarbital, and intracardially perfused with saline (0.9%) followed by paraformaldehyde (4%). Coronal slices (35 µm) were stained with cresyl-violet and imaged with conventional transmission light microscopy. Recording sites were reconstructed by comparing the images with the stereotaxic atlas of (*49*).

Data analysis and statistics

Data were analyzed in Matlab (MathWorks, Natick, MA) using the Freely Moving Animal Toolbox (M. Zugaro and R. Todorova, `http://fmatoolbox.sourceforge.net`) and custom written programs.

Identification of cell assemblies

A standard unsupervised method based on principal and independent component analyses (PCA (*16*) and ICA (*24*)) detected the co-activation of simultaneously recorded neurons. Spike trains recorded during SWS were first binned into 15-ms bins and z-scored to generate a z-scored spike count matrix Z, where $Z_{i,j}$ represents the activity of neuron i during time bin j. Principal components (PCs) were computed by eigen decomposition of the correlation matrix of Z. Principal components associated with eigenvalues exceeding the upper bound of the Marčenko-Pastur distribution were considered significant (*50*). We then carried out ICA (using the fastICA algorithm by H. Gävert, J. Hurri, J. Särelä, and A. Hyvärinen, `http://research.ics.aalto.fi/ica/fastica`) on the projection of Z onto the subspace spanned by significant PCs. Independent component (IC) weights were scaled to unit length and by convention the arbitrary signs of the weights were set so that the highest absolute weight was positive. Members of cell assemblies were identified using Otsu's method (*51*) to divide the absolute weights into two groups maximizing inter-class variance, and neurons in the group with greater absolute weights were classified as members. Goodness of separation was quantified using Otsu's effectiveness metric, namely the ratio of the inter-class variance to the total variance. This procedure yielded a set of vectors C_i representing the detected cell assemblies.

In theory, it is possible to observe an assembly with both positive and negative weight members ('mixed-signs' assemblies), representing two groups of anti-correlated neurons that inhibit each other. However, in our dataset mixed-signs assemblies were composed of more numerous members with lower separation quality compared to same-sign assemblies (Fig. S13), suggesting that mixed-signs assemblies may result from limitations of the ICA method to identify independent components from the PCs (*24*). We therefore discarded mixed-signs assemblies from further analyses.

Peer prediction

Population coupling of assembly members was verified by quantifying to what extent the spiking activity of one member could be predicted from the spiking activity of all other members (*14*). For cross-validation, spike trains were divided into two non-overlapping partitions. Using one partition ('training set'), for each assembly member i, a generalized linear model (GLM) was trained to predict its activity Z_i from the activity of all other members of the same assembly. To test performance, the GLM prediction error was computed on the remaining partition ('test set'). This procedure was repeated exchanging the training and testing sets, resulting in two-fold cross-validation. The quality of the prediction was assessed by comparing the median prediction error e to the median error $e_{shuffled}$ obtained by shuffling 50 times the predictions relative to the observed activity Z_i. The prediction gain g was defined as $g = e_{shuffled}/e - 1$ (*52*).

Assembly activations

To study downstream responses to assemblies, we computed an instantaneous assembly activation strength:

$$A_i(t) = z_i(t)^{\mathsf{T}}.f(C_i^{\mathsf{T}}.C_i).z_i(t)$$

where C_i contains the weights of the members of the i^{th} assembly, and $z_i(t)$ is the activity of the assembly members at time t (computed using 15-ms windows and a 1-ms sliding window), and $f(C_i^{\mathsf{T}}.C_i)$ is a transformation of the outer product where the diagonal is set to 0, so that spiking in a single neuron does not contribute a high activation strength. Note that only the activity of assembly members were used in this computation to ensure that the activation strength reflects periods of coactivity of the assembly members rather than global fluctuations in the activity of cells with low weights (see Fig. S14). Assemblies were considered to be active when their activation strength exceeded a threshold of the 95th percentile of the values above baseline (the median, corresponding to empty bins). The midpoint of each threshold-exceeding activation was taken as assembly activation peak for further analyses.

Downstream responses to cell assemblies

For each candidate reader cell i, we computed the peri-event time histogram (PETH) of its spikes in the 2 s interval (10 ms bins) centered on assembly activation peaks. PETHs with fewer than 30 spikes were discarded. To make computations tractable, candidate assembly–reader pairs were pre-selected for further analyses if the z-scored response exceeded 2 SDs in the 10–30 ms window following assembly activations (corresponding to the ∼20-ms conduction delay between these structures (*30*)). For each candidate assembly–reader pair, the response matrix was shuffled 200 times to determine pointwise and global confidence intervals (*15*). The pair was retained for further analysis if the following criteria were met: 1) the PETH was significant in at least one bin within the 10–30 ms window (crossing both the global and pointwise bands), and 2) the mode of the PETH was positive (the reader was activated after the assembly).

Supralinearity of reader responses to assembly activations

To assess the supralinearity of reader responses to assembly activations, we first estimated the response that could be expected from a hypothetical reader responding independently to individual assembly members. To this end, we trained a generalized linear model (GLM) to predict the reader activity around assembly member spikes outside of assembly activations:

$$R^{out}_{\Delta t} = W_{\Delta t}\ N^{out}$$

where N^{out} is a $(m+1)$-by-n^{out} matrix containing the spike counts of each of the m assembly members (plus one constant term) in 15-ms bins around each of the n^{out} assembly member spikes outside assembly activations, and $R^{out}_{\Delta t}$ is a 1-by-n^{out} vector containing the number of spikes of the reader neuron with a delay Δt around each of the n^{out} spikes; $W_{\Delta t}$ is a 1-by-$(m+1)$ vector containing the weights of the GLM fit for delay Δt (Δt varies between −1 s and 1 s) to produce the curves in Fig. 2. This linear model therefore captured the response of the reader at delay Δt if the reader were responding to each individual assembly member independently. To estimate what the response of such a linear reader would be during assembly activations, we computed:

$$\eta_{\Delta t} = w_{\Delta t}\, N^{in}$$

where N^{in} is a $(m+1)$-by-n^{in} matrix containing the spike counts of each of the m assembly members (plus one constant term) in 15-ms bins around each of the n^{in} assembly member spikes emitted during assembly activations, and $\eta_{\Delta t}$ is the activity predicted by the model for delay Δt. Thus, the *collective* impact of the upstream assembly (beyond the sum of individual contributions) would be reflected in reader responses beyond $\eta_{\Delta t}$. We quantified this supralinearity by computing:

$$S_{\Delta t} = \frac{R^{in}_{\Delta t} - \eta_{\Delta t}}{\eta_{20\text{ms}}}$$

where $R^{in}_{\Delta t}$ is a 1-by-n^{in} vector containing the number of spikes of the reader neuron with a delay Δt around each of the n^{in} spikes, $\eta_{20\text{ms}}$ is a normalisation factor corresponding to the estimated linear response $\eta_{\Delta t}$ at $\Delta t = 20$ ms, and $S_{\Delta t}$ is the reader supralinearity at delay Δt.

Simulated readers To estimate the supralinearity that would be expected from readers selective to collective activity vs unresponsive to collective activity, we repeated the above analyses on simulated data. We first simulated a 'perfect' reader that responded exclusively to the collective activity of the assembly: it only fired 20 ms after each partial activation recruiting at least half of the largest subset of co-active members (see *Pattern Completion* section below). We then simulated an 'independent' reader which fired 20 ms after every spike emitted by an assembly member, regardless of any collective activity.

Time scales The above analysis used a time scale of 15-ms for cell assemblies (Fig. 2 and Fig. S5). We repeated this analysis for multiple time scales (Fig. S7). Cell assemblies were detected as described above, but using time bins of 1 ms, 5 ms, 10 ms, 15 ms, 20 ms, 25 ms, 30 ms, 40 ms, 50 ms, 75 ms, and 100 ms. One critical issue with this analysis is that larger time bins may contain assemblies expressed at faster time scales: for instance, a 15-ms assembly also fits (and could thus also be detected) in time bins of e.g. 30 ms or 100 ms — actually, in any time bin larger than 15 ms. To ensure that the analysis for a given time scale only used assemblies specifically expressed at that time scale, we excluded all epochs that contained activations of the same assembly at briefer time scales. The remaining activations were used to split member spikes between n^{in} (assembly member spikes emitted during assembly activations) and n^{out} (assembly member spikes emitted outside assembly activations). The two response curves (R^{in} and η) were normalized conjointly: they were concatenated into a single vector for z-scoring.

Selectivity to identity of assembly members

To test whether the reader was sensitive to the co-activation of multiple assembly members, rather than simply responding to the total spike output of assembly members, we compared the reader activity around co-activations of two different assembly members ('AB') to the reader activity around the repeated activation of a single assembly member ('AA').

For each assembly, we considered every possible permutation of two members. Each of these permutations was analyzed independently, and from herein, the two neurons in a given permutation are termed 'A' and 'B'. To find 'AB' events, we performed a search in the inter-spike intervals of 'A' and 'B', retaining pairs of spikes emitted by the two neurons within the assembly time scale (15 ms). To find a matching set of 'AA' events, we performed an equivalent search of moments when neuron 'A' emitted two consecutive spikes within the same time scale (15 ms). Permutations in which we found less than 20 'AB' events or less than 20 'AA' events were discarded from further analyses. We computed a peri-event time histogram (PETH) of the firing rate of the reader neuron around 'AB' and 'AA' events, using the midpoint of the two spikes ('AB' or 'AA') as a reference. The two PETHs were normalized conjointly: they were concatenated into a single vector for z-scoring.

The above analysis used a time scale of 15-ms (Fig. S6). We repeated the analysis for multiple time scales (Fig. 2, Fig. S8). Cell assemblies were detected as described above, but using bins of 1 ms, 5 ms, 10 ms, 15 ms, 20 ms, 25 ms, 30 ms, 40 ms, 50 ms, 75 ms, and 100 ms. For each time scale, we detected candidate readers using the procedure outlined above. We further subdivided reader responses according to the delay between the two spikes, within a precision of 5 ms. For example, to compute the reader response to 'AA' events with a delay of 45 ms, we retained 'AA' events for which the two consecutive spikes were within 42.5–47.5 ms of each other (without any 'A' or 'B' intervening spikes during this interval).

Pattern Completion

To quantify pattern completion, we determined the average reader responses to activation of all possible combinations of assembly members. For example, for assembly 'ABCD', we measured reader responses to the (complete) 4-member assembly activations 'ABCD', to each of the 3-member (incomplete) activations 'ABC', 'ABD', 'ACD', 'BCD', to each of the 2-member (incomplete) activations 'AB', 'AC', 'AD', 'BC', 'BD', 'CD', and to each of the single-member (incomplete) activations 'A', 'B', 'C', 'D', relative to the baseline reader firing rate in all sleep periods. For each assembly–reader pair, we fit the resulting responses with a sigmoid curve:

$$F_\sigma(x) = \frac{1}{1 + e^{-k(x - x_0)}}$$

where x is the proportion of active assembly members, and x_0 and k are the model parameters corresponding to the midpoint and the steepness of the curve, respectively. To estimate the goodness-of-fit, we computed

$$R^2_\sigma = 1 - \frac{\sum_i (r_i - F_\sigma(n_i/n))^2}{\sum_i (r_i - \bar{r})^2}$$

where r_i is the reader response to combination i, and n_i/n is the proportion of active members. We likewise estimated the goodness-of-fit of a proportional response $F_\alpha(x) = r_{complete}\ x$, where $r_{complete}$ is the reader response to activations of the complete assembly (or of the largest subset of co-active members):

$$R^2_\alpha = 1 - \frac{\sum_i (r_i - F_\alpha(n_i/n))^2}{\sum_i (r_i - \bar{r})^2}$$

Finally, we quantified the boost in observed response relative to the proportional response as the gain $r - F_\alpha$. We split the data in tertiles according to x such that $x_1 \in (0, 1/3]$, $x_2 \in (1/3, 2/3]$, and $x_3 \in (2/3, 1]$ and tested each tertile for significant pattern completion.

Pattern Separation

To assess how readers discriminated between different assemblies, we first determined the response of each neuron j following activations of each recorded assembly i, and computed the Hoyer coefficient of sparsity:

$$H_j = \frac{\sqrt{n} - \frac{\sum_i^n r_{ij}}{\sum_i^n (r_{ij})^2}}{\sqrt{n} - 1}$$

where n is the number of assemblies recorded simultaneously with neuron j, and r_{ij} is the response of neuron j to assembly i. As neurons with lower baseline firing rates tend to have larger Hoyer coefficients of sparsity, to compare across neurons we measured sparsity relative to surrogate data, where assembly identities were shuffled across all pooled assembly activations (i.e., an activation of assembly a was randomly assigned to assembly b). For each reader, we repeated this procedure 1000 times and computed the mean Hoyer coefficient of the shuffled data H^0_j. The sparsity increase relative to the shuffled data was defined as:

$$H^{increase}_j = \frac{H_j - H^0_j}{H^0_j}$$

To determine whether reader responses were particularly sparse, we compared sparsity increases between readers and non-readers (neurons for which a paired assembly could not be detected) using the Wilcoxon rank sum test.

To test whether readers could discriminate between similar patterns, for each reader–assembly pair we sought a second assembly with multiple overlapping members (at least 25% of each assembly and > 2 members, e.g. 'ABCD' and 'ABE'; varying the number of overlapping members did not change our results: see Supplementary Figure 11), and defined the discrimination index between the two assemblies as:

$$d = \frac{r_1 - r_2}{r_1 + r_2}$$

where r_1 is the reader response to its paired assembly, and r_2 is its response to the overlapping assembly. To test for significant discrimination, we computed discrimination indices for surrogate data, where the activations of the two assemblies were pooled and the assembly identities were shuffled. This was repeated 1000 times, and when the discrimination index of a reader exceeded those of 95% of the shuffles, the reader was considered to perform pattern separation.

Behavioral testing

Behavioral testing only relates to results shown in Fig. 4 and Fig. S12 as all other analyses were performed using data from pre-training sleep sessions, i.e. preceding any exposure to the protocol described here.

The animals were tested in a slightly extended version of the standard fear conditioning and extinction paradigm, initially intended to discriminate between cued and context fear learning. However, only

context extinction yielded useful data for the current study and is reported here. Briefly, fear conditioning took place in one chamber (context), where foot shocks were associated with auditory stimuli (conditioned stimuli, CS). Extinction took place either in the same chamber without the CS (contextual extinction), or in a different chamber with the CS (cued extinction). Daily recording sessions consisted of two 37-min exposure sessions (one per chamber), preceded, separated, and followed by sleep sessions of 2-3 hours. Only sleep periods before and after exposure to the conditioning chamber were analyzed here, amounting to two pre-training control sessions, two fear conditioning sessions, and two extinction sessions per animal.

The conditioning chamber was cubic (side length, 40 cm) with gray plexiglass walls lined with ribbed black rubber sheets and a floor composed of nineteen stainless steel rods (0.48 cm diameter, 1.6 cm spacing) connected to a scrambled shock generator (ENV-414S, Med Associates, USA). It was mildly scented daily with mint-perfumed cleaning solution (Simple Green, Sunshine Makers). A custom-made electronic system presented the animals with two auditory CS (80 dB, 20 s long, each composed of 1 Hz, 250 ms long pips of either white noise, CS+ paired to shocks, or 8 kHz pure tones, CS- unpaired). These auditory stimuli (8 CS+ and 8 CS-) were presented starting at $t = 3$ min, separated by random-duration inter-trial intervals (120–240 s). Foot shocks consisted in shocks scrambled across floor rods (1 s, 0.6 mA, co-terminating with CS+ presentations; CS+ and CS- were presented in pseudorandom order allowing no more than 2 consecutive presentations of the same-type CS). Sleep was recorded in a cloth-lined plastic flowerpot (30 cm upper diameter, 20 cm lower diameter, 40 cm high).

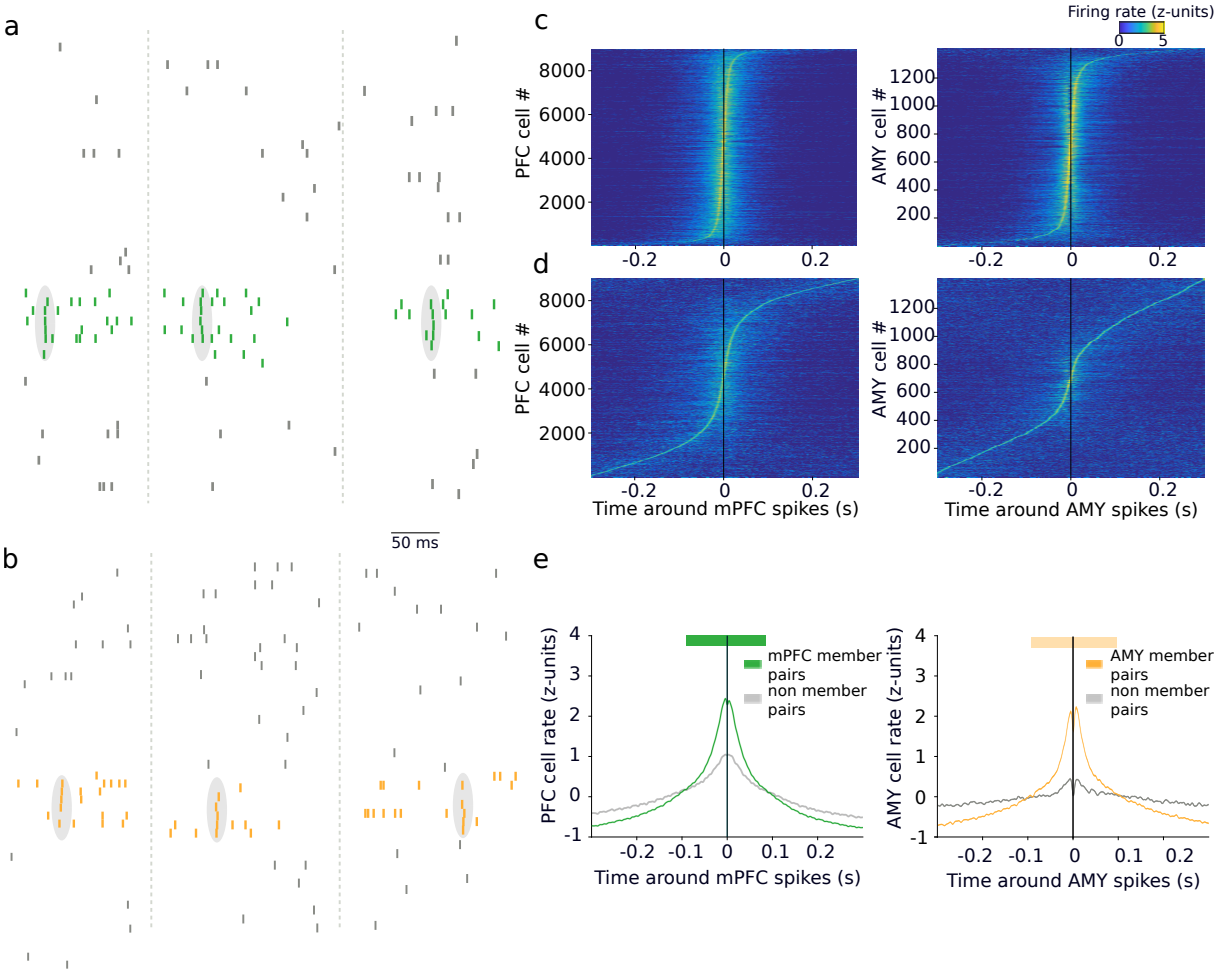

Fig. S1. Cell assemblies in the cortico-amygdalar circuit. **a**, Spike trains of a subset of 35 simultaneously recorded units in prefrontal cortex during sleep (rasters: action potentials; gray ellipses surrounding colored ticks: co-activation events). **b**, Spike trains of a subset of 30 simultaneously recorded units in the amygdala during sleep (rasters: action potentials; gray ellipses surrounding colored ticks: co-activation events). **c**, Z-scored cross-correlations between members of the same prefrontal (left) and amygdalar (right) assemblies, ordered by mode. **d**, Same as in (**c**) for control pairs, illustrating that fewer pairs have modes at brief delays. **e**, Averages of (**c**) (colored curves) and (**d**) (gray curves). Members of the same assemblies had significantly higher synchrony at short delays than control pairs (thick horizontal colored bars: $p<0.05$, Monte-Carlo bootstraps).

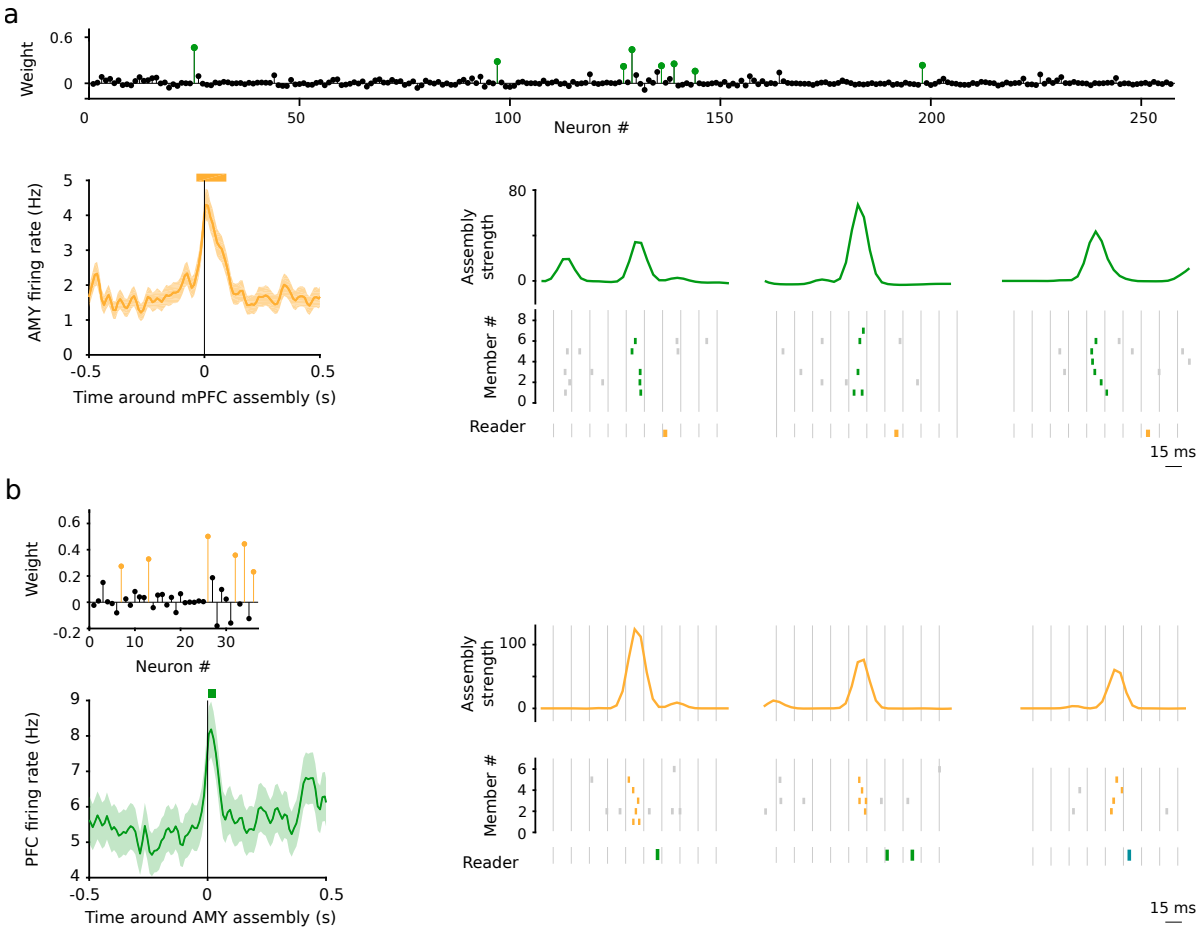

Fig. S2. Example assembly–reader pairs. **a**, Activations of a prefrontal assembly closely followed (10–30 ms) by significant responses of an amygdalar neuron. Top: cell assembly weights (colored circles: assembly members, black circles: non-members). Bottom left: firing rate of an amygdalar neuron centered on all prefrontal assembly activations (mean ± s.e.m.). Thick orange horizontal bar indicates significant responses ($p<0.05$: Monte-Carlo bootstrap test; see Methods). Bottom right: example assembly activations (green curves: activation strength) followed by downstream spiking (rasters: prefrontal spikes within (green) or outside (gray) epochs of assembly activation; orange rasters: amygdalar spikes). Reader responses occurred ∼20 ms after assembly activations. **b**, Same as (**a**) for an amygdalar assembly and a downstream prefrontal neuron.

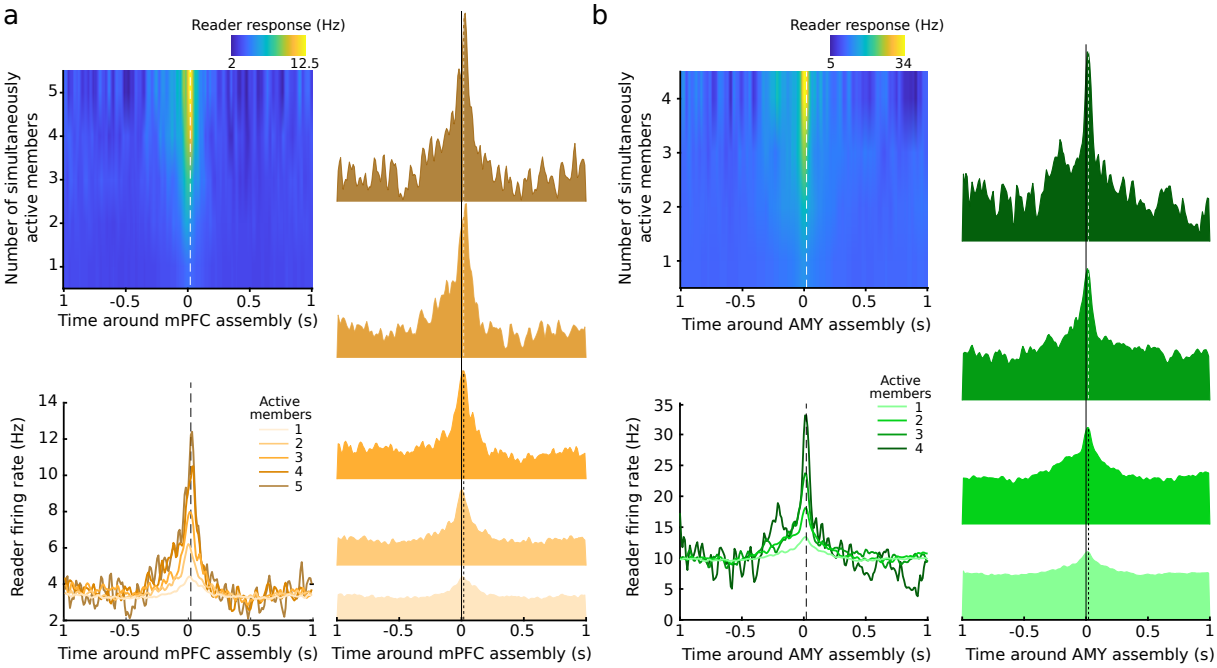

Fig. S3. Assembly members exert a synergistic influence on their targets: reader response rate increases with the number of co-active assembly members. **a**, Example amygdalar response to increasing numbers of simultaneously active prefrontal assembly members. Top left: Reader firing rate centered on assembly activation. Right: Reader firing rate for different numbers of co-active members. Bottom left: Superimposed response curves. **b**, Same as (**a**) for example prefrontal assembly and amygdalar reader.

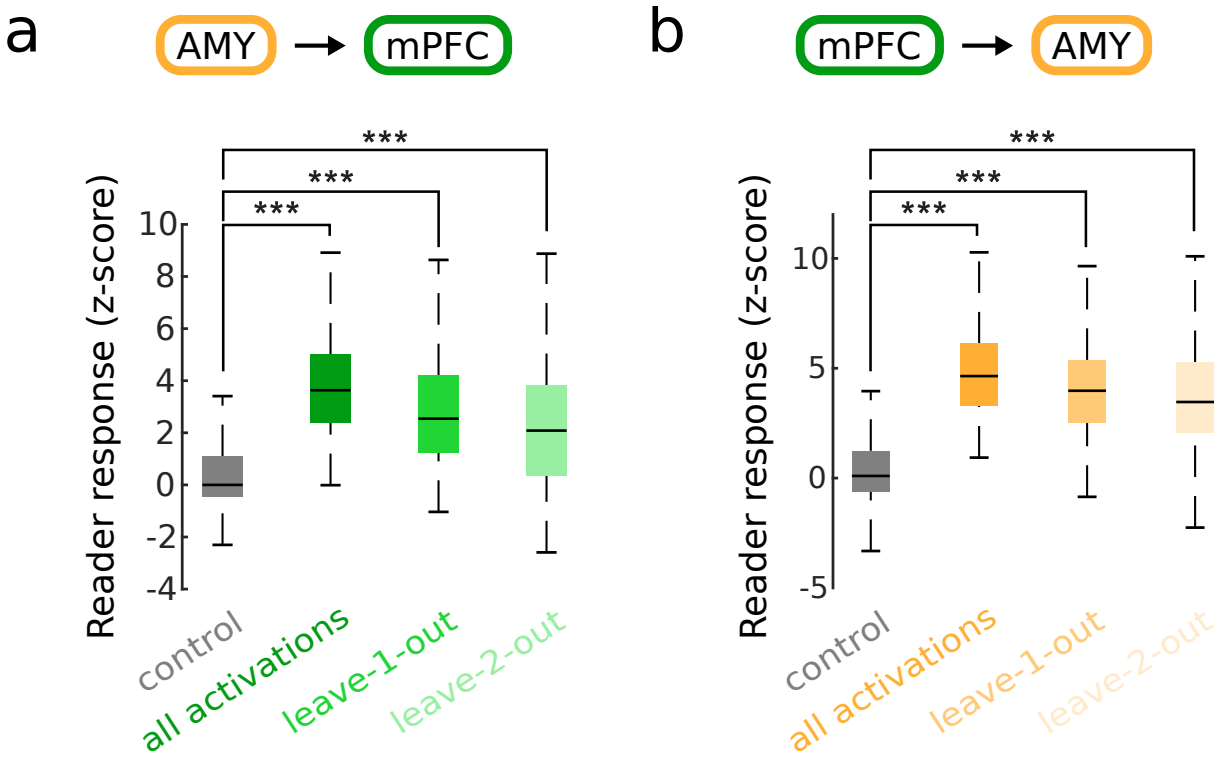

Fig. S4. Assembly members exert a synergistic influence on their targets: responses are not driven by single 'vocal' members. **a**, Average response of prefrontal readers to amygdalar assembly activations when the most effective members (i.e. the members whose spikes outside assembly activation epochs were followed by the largest response by the reader neuron at 10–30 ms) of upstream assemblies were not recruited (leave 1-out, leave 2-out). **b**, Same as (**a**) for amygdalar reader responses to member spikes of prefrontal assemblies.

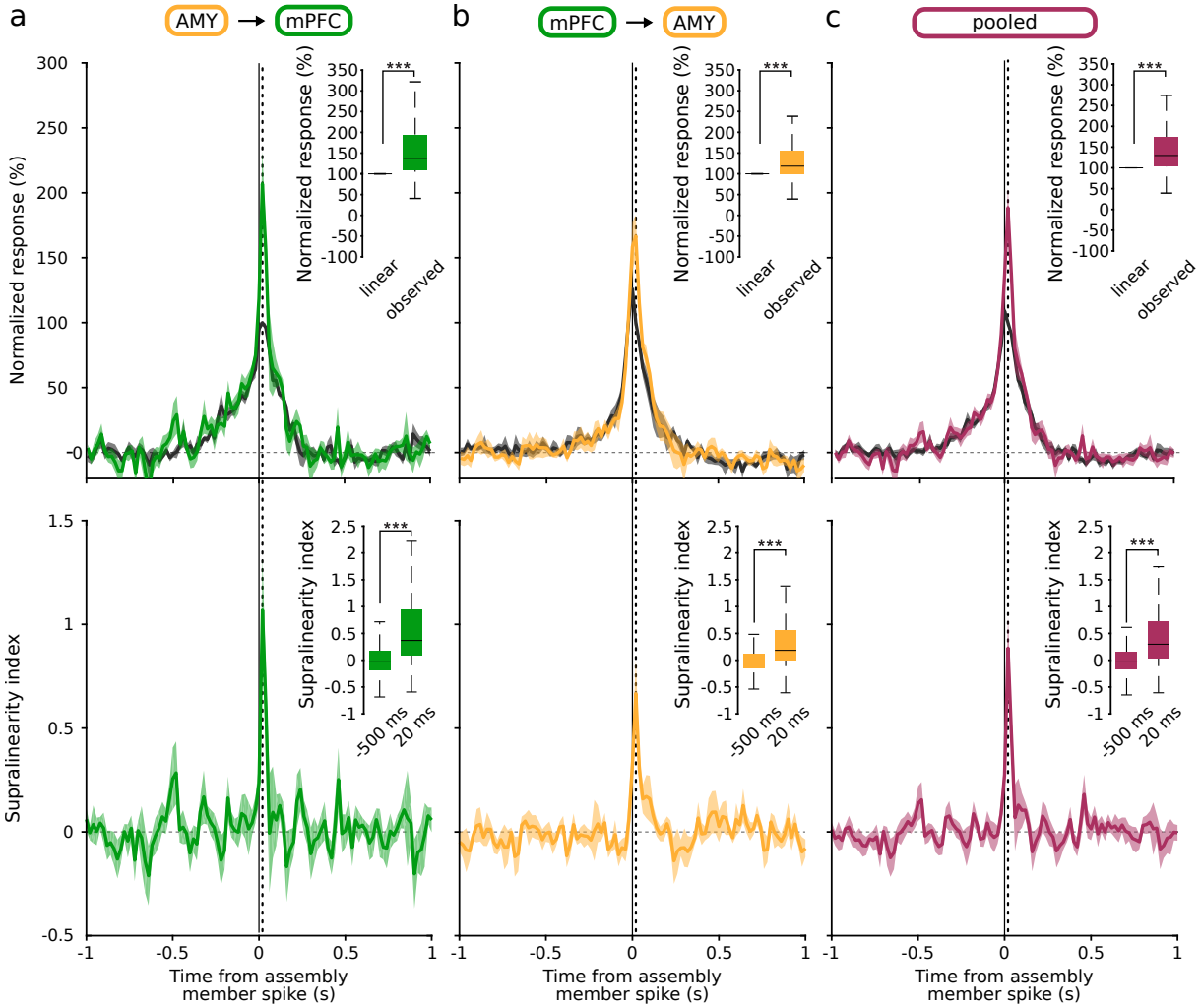

Fig. S5. Supralinearity of reader responses. **a**, Top: Observed responses (colored curve: mean ± s.e.m.) of prefrontal readers compared to the estimated response of a linear reader (gray curve: mean ± s.e.m.). Inset: The observed response was greater than the linear estimate at 20 ms (***$p<0.001$, Wilcoxon signed-rank test). Bottom: Supralinearity index of prefrontal reader responses. Dashed line: peak of reader responses to assembly activations at 20 ms. Inset: Supralinearity at 20 ms vs baseline (***$p<0.001$, Wilcoxon signed-rank test). **b**, Same as (**a**) for amygdalar reader responses to spikes of members of prefrontal assemblies. **c**, Same as (**a**) for pooled responses of both amygdalar and prefrontal readers.

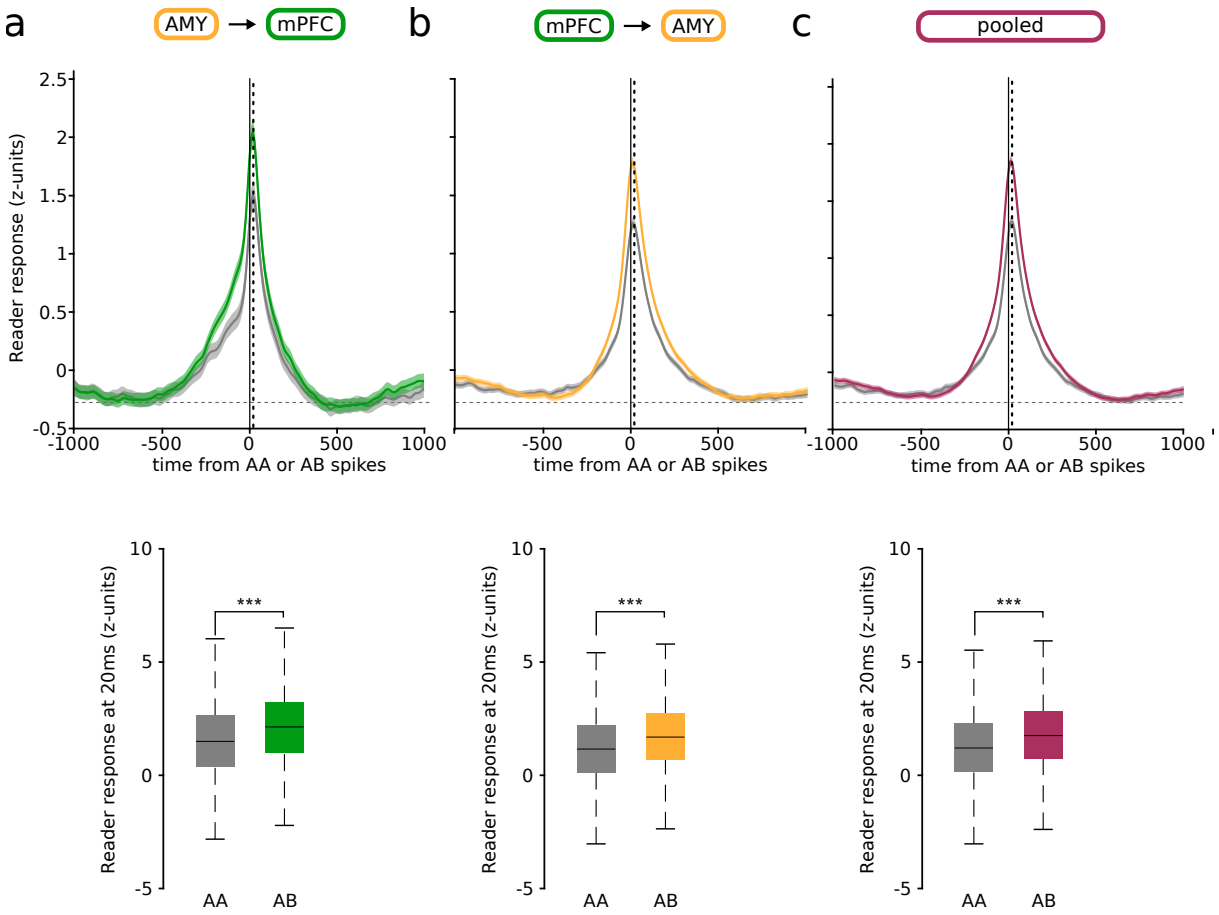

Fig. S6. The identity of participating members matters beyond their compound activity. **a**, Response of prefrontal readers to amygdalar assembly members. Top: z-scored responses of reader neurons to two spikes emitted by different assembly members (AB, colored curve), compared to the control responses to two spikes emitted by the same assembly member (AA, gray curve) (mean ± sem). Bottom: Z-scored reader responses at 20 ms (***$p<0.001$, Wilcoxon signed-rank test). **b**, Same as (**a**) for amygdalar readers and PFC assembly members. **c**, Same as (**a**) for pooled responses of both amygdalar and prefrontal readers.

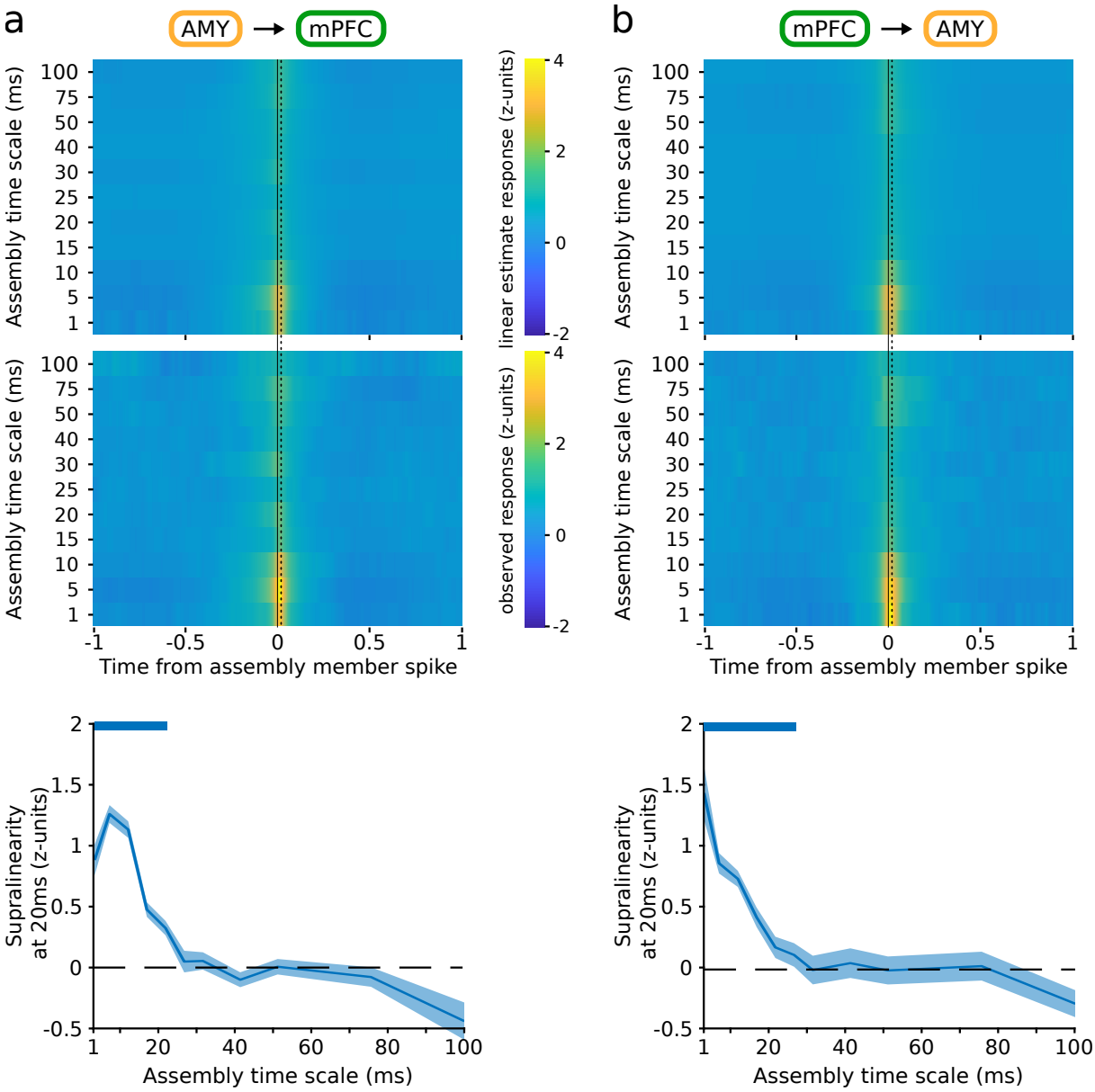

Fig. S7. Time scale of reader response supralinearity. **a**, Response of prefrontal readers to activations of amygdalar assemblies at varying time scales. Top and center: mean z-scored responses of a linear model vs the observed reader response, as a function of the time scale of the assembly. Bottom: difference between the two (observed response−linear estimate), for varying time scales. Thick colored horizontal bars indicate significant differences ($p<0.05$, Monte-Carlo bootstrap test). **b**, Same as (**a**) for amygdalar reader responses to member spikes of prefrontal assemblies. Note that in both cases, supralinearity is significantly greater than 0 for time scales up to 20–25 ms.

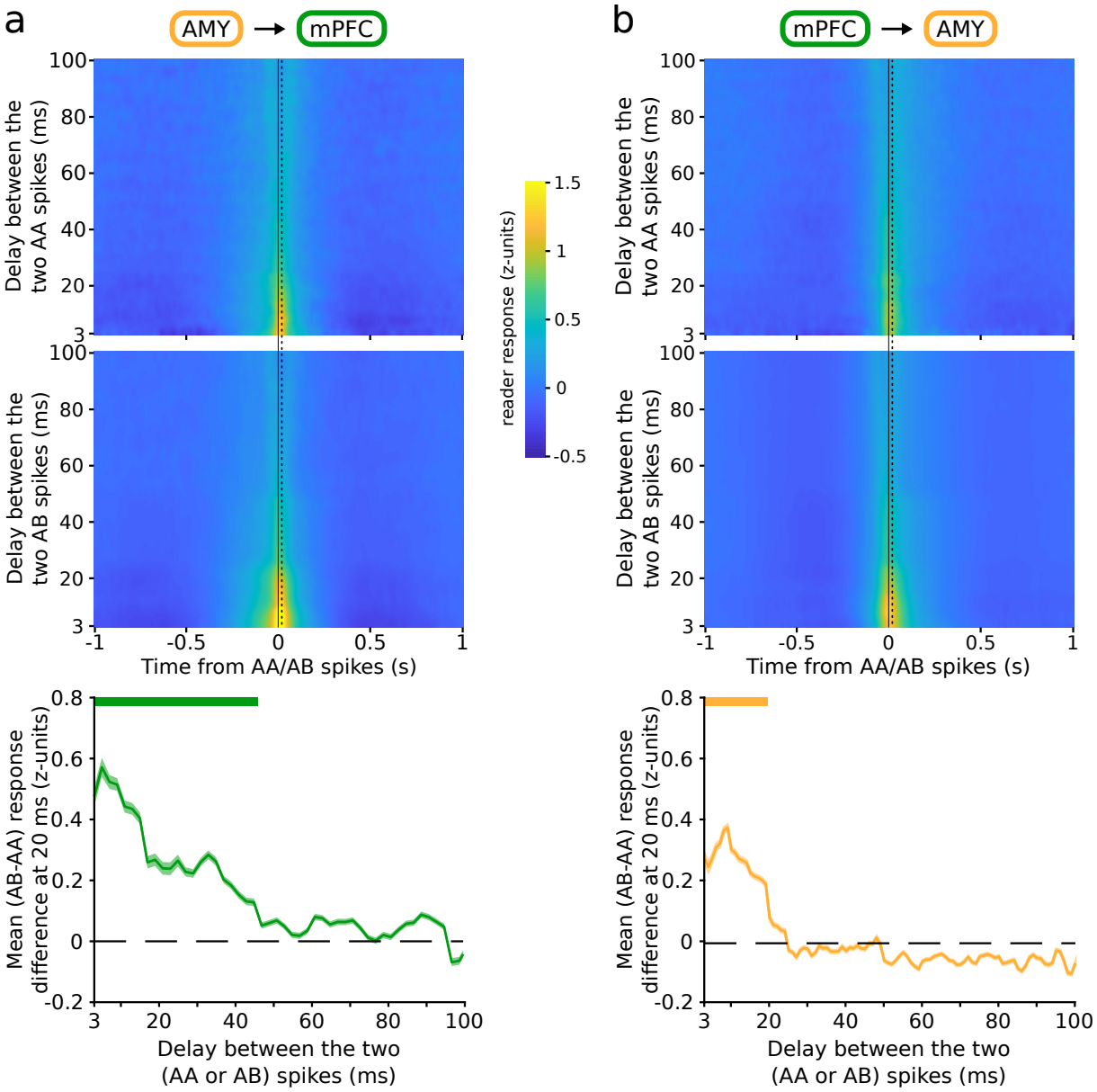

Fig. S8. Time scale of reader sensitivity to assembly member identity. **a**, Response of prefrontal readers to two spikes emitted by different assembly members (AB), compared to the control responses to two spikes emitted by the same assembly member (AA), at varying time scales. Top and center: mean z-scored responses of reader neurons to spikes emitted by the same (AA, top) vs different (AB, center) members of an upstream assembly, as a function of the temporal delay between the two spikes. Bottom: difference between the two (AB−AA), for varying temporal delays. Thick colored horizontal bars indicate significant difference ($p<0.05$, Monte-Carlo bootstrap test). **b**, Same as (**a**) for amygdalar readers.

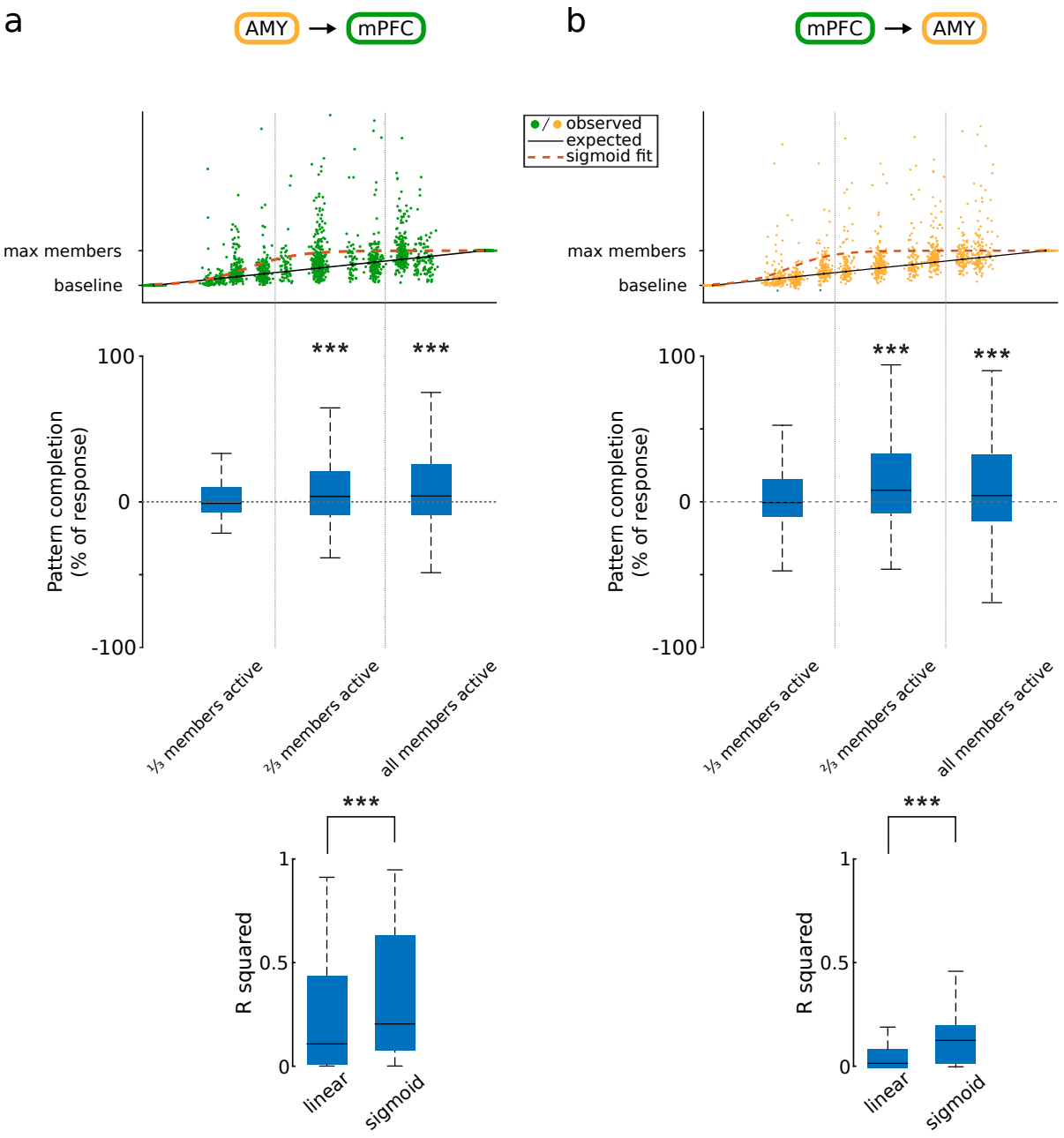

Fig. S9. The assembly–reader mechanism can implement pattern completion. **a**, Prefrontal reader responses to amygdalar assemblies. Top: Pooled reader responses as a function of the proportion of active assembly members. Black line: linear response. Dashed red curve: best-fit sigmoid curve. Center: boost in reader response (relative to a proportional response) for all assembly–reader pairs as a function of the proportion of active assembly members. The gain was significant for the second and third quantiles (***$p<0.001$, Wilcoxon signed-rank test), but not for the first quantile (*$p<0.05$, Wilcoxon signed-rank test). Bottom: The data were better fit with sigmoidal than linear models (***$p<0.001$, Wilcoxon signed-rank test). **b**, Same as (**a**) for amygdalar reader responses to prefrontal assemblies.

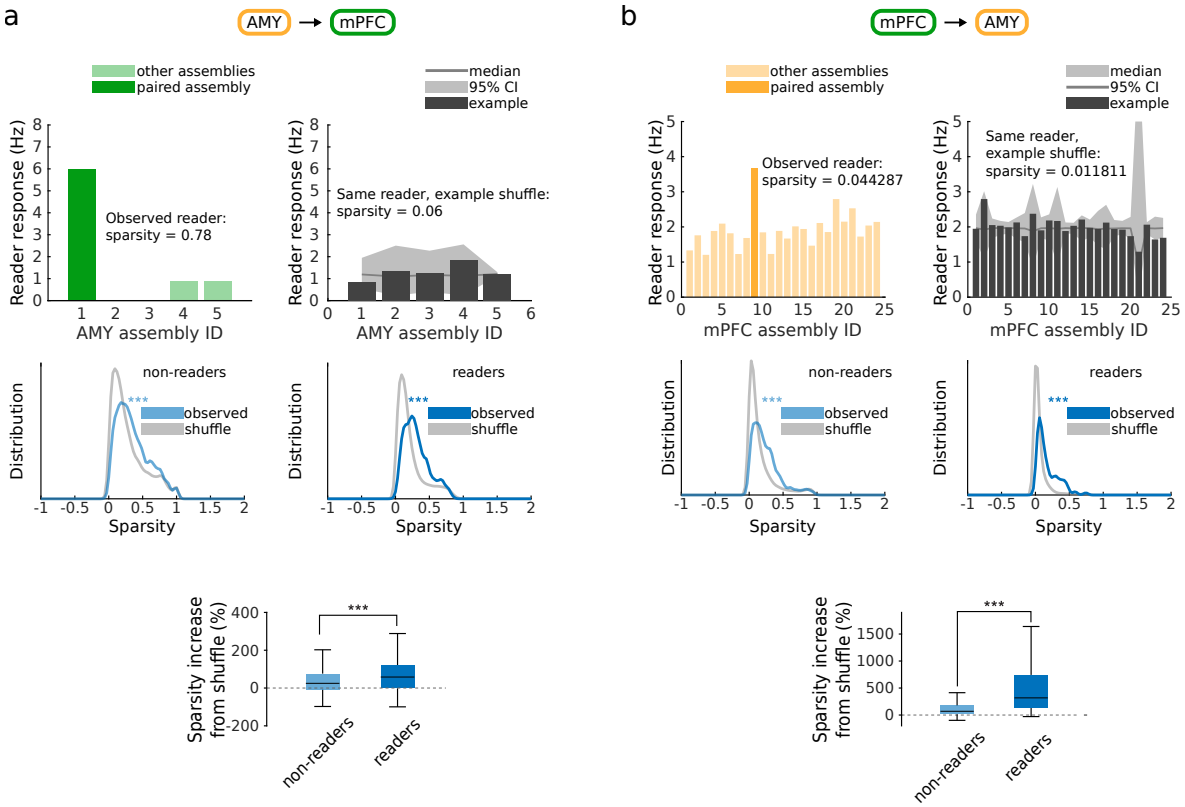

Fig. S10. The assembly–reader mechanism can implement pattern separation: reader responses are selective for specific assemblies. **a**, Sparsity of prefrontal reader responses to amygdalar assemblies. Top left: Responses of an example prefrontal neuron to each amygdalar cell assembly in the recording session. Responses are selective for the paired assembly (dark green), compared to other assemblies (light green). Top right: Control responses of the same prefrontal neuron to surrogate assembly activations (shuffled assembly identities) are not selective. Center: distribution of sparsity for non-reader (left) and reader (right) neurons, compared to control sparsity computed from shuffled data (gray). Note that the observed responses are sparser than the shuffled control (***$p<0.001$, Wilcoxon signed rank test). Bottom: Sparsity increase from shuffle, for reader vs non-reader neurons (***$p<0.001$, Wilcoxon rank sum test). **b**, Same as (**a**) for amygdalar reader responses to prefrontal assemblies.

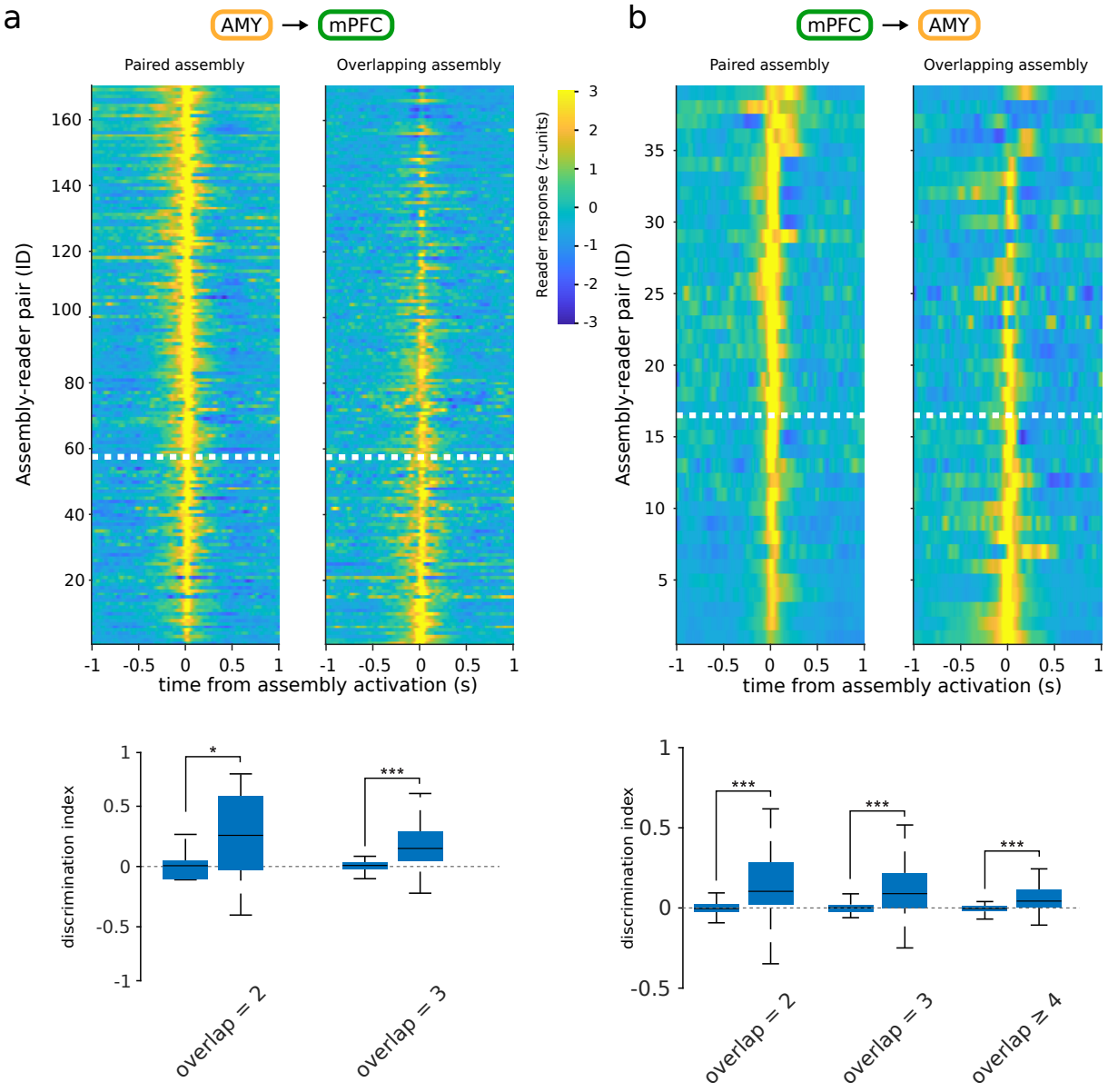

Fig. S11. The assembly–reader mechanism can implement pattern separation: readers can discriminate between overlapping assemblies. **a**, Pattern separation in prefrontal reader responses to amygdalar assemblies. Top: prefrontal reader responses to activation of a paired assembly (left) vs a different but overlapping ($\geq$25%) assembly, sorted by discrimination index. Responses above the white dotted line manifested significant pattern separation (greater discrimination indices than shuffled data, $p<0.05$, Wilcoxon rank sum test). Bottom: Discrimination indices were greater for observed than shuffled data (***$p<0.001$, Wilcoxon rank sum test). **b**, Same as (**a**) for amygdalar reader responses to prefrontal assemblies.

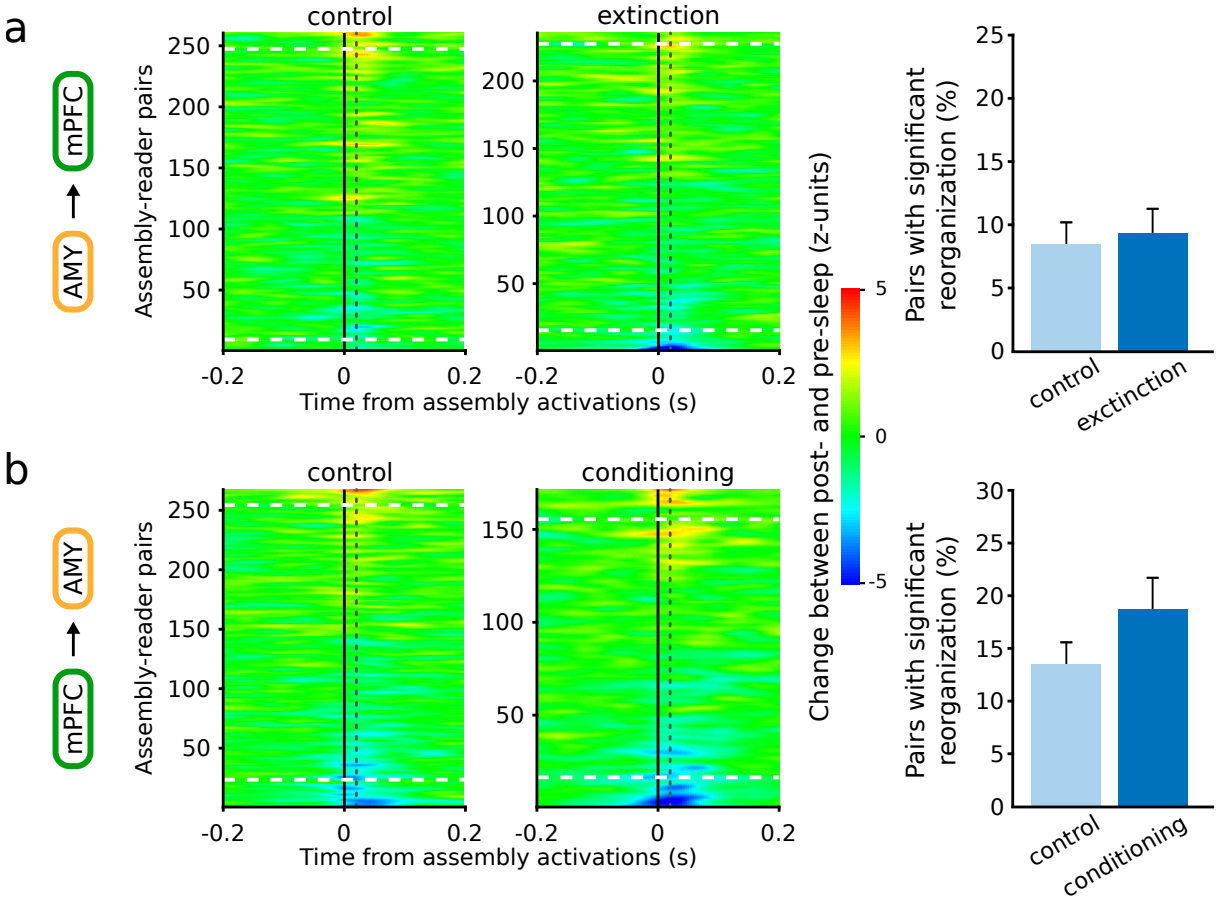

Fig. S12. Functional selectivity of learning-related changes in assembly–reader pairs. **a**, Changes in prefrontal reader responses between sleep following and sleep preceding fear extinction vs control sessions, centered on amygdalar assembly activations. Responses are sorted according to change in response. Assembly–reader pairs below the lower dashed line significantly decreased their responses, and assembly–reader pairs above the upper dashed line significantly increased their response in post-learning sleep ($p<0.05$, Monte-Carlo bootstrap tests). Right: the number of assembly–reader pairs that significantly changed their responses ($p<0.05$, Monte-Carlo bootstrap test) was not greater after fear extinction than after control sessions ($p>0.05$, chi-square test). **b**, Same as (**a**) for changes in amygdalar reader responses to prefrontal assemblies in sleep following and sleep preceding control vs fear conditioning sessions. Right: the number of assembly–reader pairs that significantly changed their responses ($p<0.05$, Monte-Carlo bootstrap test) was not greater after fear conditioning than after control sessions ($p>0.05$, chi-square test).

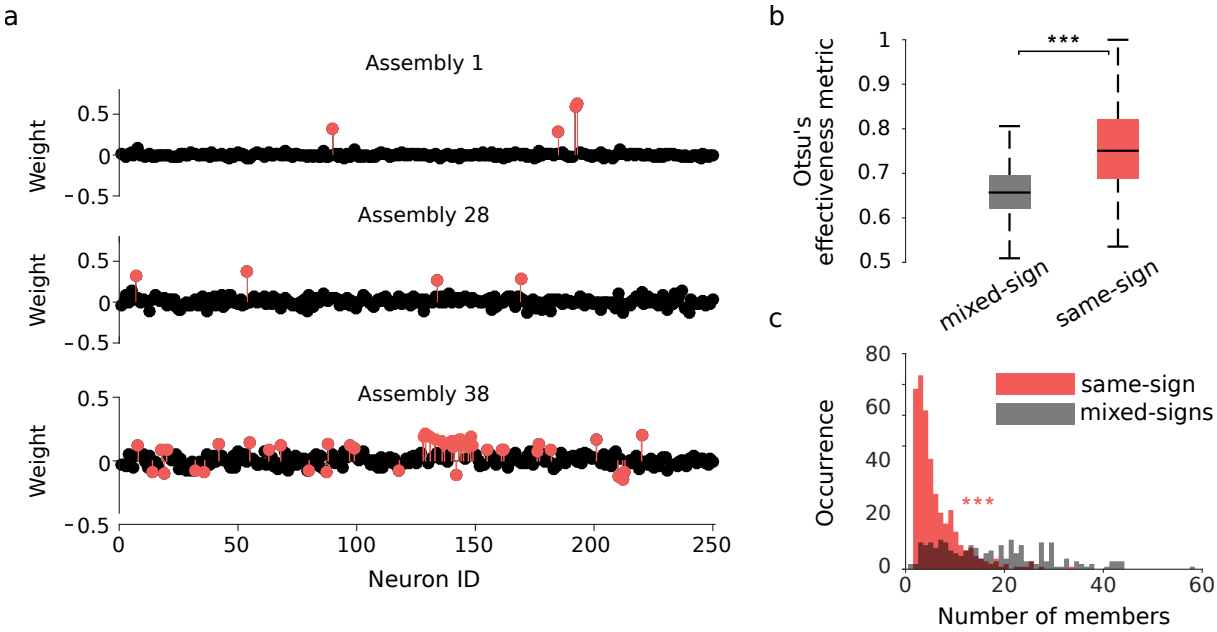

Fig. S13. Selection of cell assemblies with same-sign component weights. **a**, Cell assembly weights of three representative prefrontal assemblies (colored circles: assembly members, black circles: non-members), corresponding to eigenvalues 1, 28 and 38. Whereas all members of assemblies 1 and 28 were of the same (positive) sign, assembly 38 included members with both positive and negative weights ('mixed-sign assembly'). **b**, The separation between members and non-members was significantly better in same-sign assemblies than mixed-sign assemblies (***$p<0.001$, Wilcoxon rank sum test). **c**, Mixed-sign assemblies had significantly more members than same-sign assemblies (***$p<0.001$, Wilcoxon rank sum test).

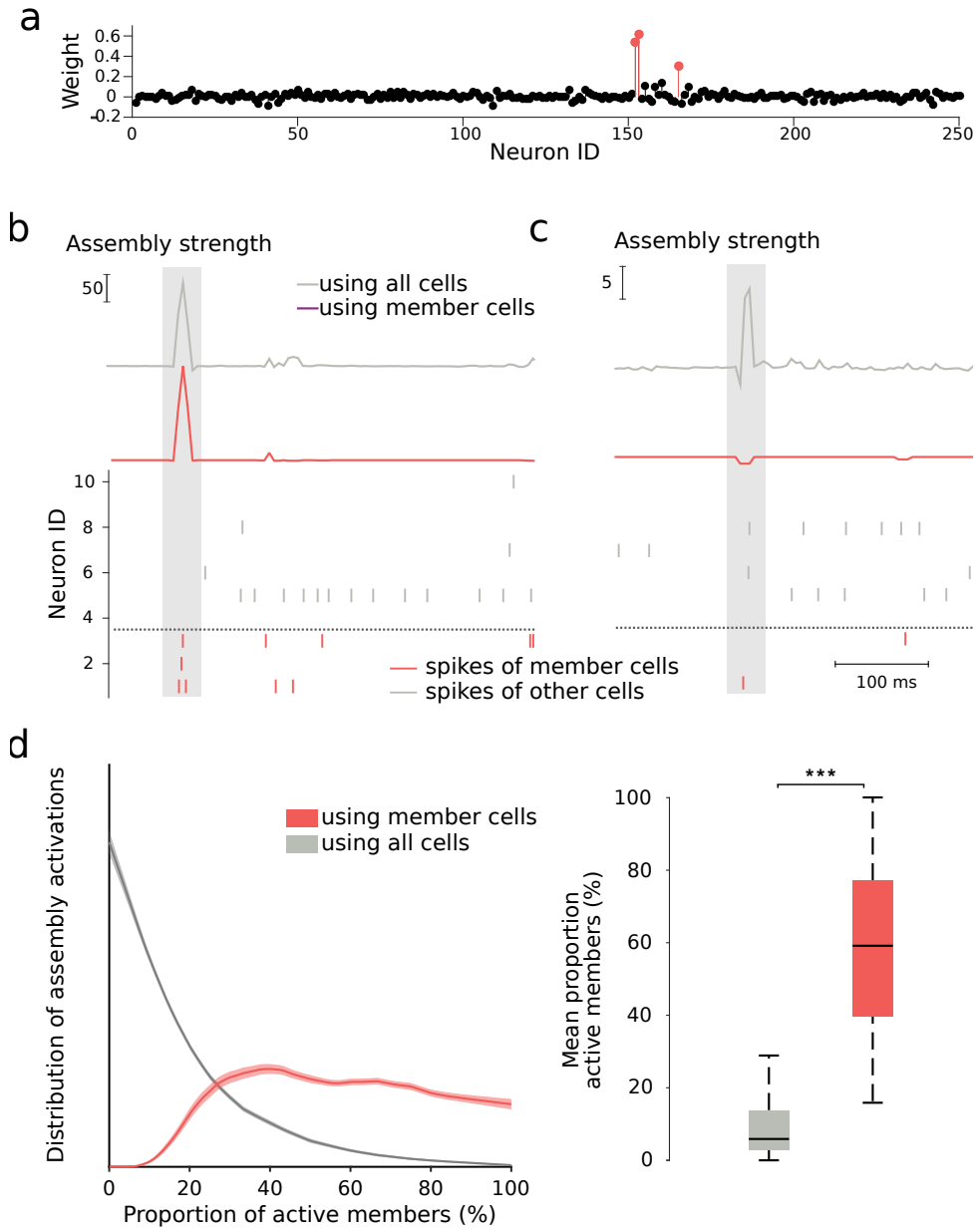

Fig. S14. Computation of assembly activation strength. **a**, An example assembly recorded in the prefrontal cortex. Red dots: assembly members. **b**, Example activation of assembly shown in (**a**). Top: Assembly activation strength computed using either the activity of all cells (gray curve) or the activity of member cells only (red curve). Bottom: Raster plot of the activity of a representative subset of neurons, ordered by absolute weight (vertical ticks: action potentials; red ticks: member cells; gray ticks: non-member cells; shaded rectangle: putative assembly activation). All three members were active, resulting in a high activation strength in both curves. **c**, Same as (**b**) but for an instance in which only a single assembly member was active, at the same time as two non-members. The corresponding peak in the gray curve would result in incorrect detection of an activation of the assembly. This spurious peak is absent from the red curve, where activity strength is computed using only assembly members. **d**, Left: Proportion of assembly members co-active around peaks in the assembly activation strength computed using the activity of member cells only (red) or using the activity of all cells (gray). Right: using the activity of member cells results in detection of assembly activation events with greater proportions of co-active members (***$p<0.001$, Wilcoxon signed rank test)).